

Impact assessment of a wind turbine blade root during an offshore mating process

Amrit Shankar Verma^{a,b}, Zhiyu Jiang^{b,c,*}, Nils Petter Vedvik^d, Zhen Gao^{a,b,e}, Zhengru Ren^{a,b,e}

^a*Department of Marine Technology, Norwegian University of Science and Technology (NTNU), Norway*

^b*Centre for Marine Operations in Virtual Environments (SFI MOVE), NTNU, Norway*

^c*Department of Engineering Sciences, University of Adger, 4879 Grimstad, Norway*

^d*Department of Mechanical and Industrial Engineering, NTNU, Norway*

^e*Centre for Autonomous Marine Operations and Systems (SFF AMOS), NTNU, Norway*

Abstract

Single-blade installation is a popular method for installing blades on bottom-fixed offshore wind turbines. A jack-up crane vessel is often employed, and individual blades with their roots equipped with mechanical joints and bolted connections are lifted to the tower-top height and mated with a pre-assembled hub. The final mating phase is challenging and faces significant risks of impact. Due to relative motions between the blade and the hub, substantial impact forces may arise and lead to severe structural damages at root connections, thereby causing delays in the installation task. The present paper considers a realistic scenario of the mating process and investigates the consequences of such impact loads. Here, a single-blade model with tugger lines and a monopile model were established using a multi-body formulation, and relative velocities under collinear wave and wind conditions were obtained. A three-dimensional finite element model was developed for the blade root with T-bolt connections, and an impact investigation was performed for the case in which a guiding connection impacts the hub. The results show severe bending and plastic deformation of the guide pin bolt together with failure of the adjoining composite laminate at the root connection. Based on the type of damage obtained for the different environmental conditions considered, this paper also discusses its consequence on the installation tasks and suggests onboard decision making in case of an impact incident. The results of this study provide new insights regarding the mating phase and can be utilised to establish response-based operational limits.

Keywords: Offshore wind turbine blade, mating phase, jack-up vessel, monopile, impact loads,

*Corresponding author

Email addresses: amrit.s.verma@ntnu.no (Amrit Shankar Verma), zhiyu.jiang@uia.no (Zhiyu Jiang), nils.p.vedvik@ntnu.no (Nils Petter Vedvik), zhen.gao@ntnu.no (Zhen Gao), zhengru.ren@ntnu.no (Zhengru Ren)

wind excitations, T-bolt connections, marine operations.

1. Introduction

1 The constant need for renewable sources of energy has increased the demand for wind turbines,
2 both in the onshore and offshore sectors [1, 2]. In addition, the favourable factors in the offshore
3 environment, such as the distant location of turbines from human settlements, large space to
4 deploy big turbines and the possibility to transport them on barges, make offshore turbines more
5 attractive than land-based turbines. Consequently, the rated capacity of offshore wind turbines
6 has increased at a rate of 102% over the past decade, with monopile-type offshore wind turbines
7 accounting for more than 87% of the total installed turbines in the European market [3, 4].

8 The recent report [5] from the European Wind Energy Association suggests that by 2050,
9 offshore wind energy could exceed the total onshore wind energy capacity [5, 6, 7]. However,
10 achieving this goal would require turbines with rated power capacities that are larger than those of
11 the existing turbines to be installed in deeper waters and far away from the shore. Note that in the
12 year 2017 alone, the average rated capacity of all the offshore wind turbines that are grid connected
13 in European waters was 5.9 MW [4] along with turbines with rated capacities reaching 8 MW. The
14 recently announced Haliade-X 12 MW class of offshore wind turbines by General Electric (GE)
15 will have blades that are 107 m long and that are mounted at a hub height of approximately 260
16 m above the mean sea level [8]. One of the main objectives for this class of turbines is to reduce
17 the number of turbine units in an offshore farm. This presents less outflow of the capital on the
18 overall balance of the plant [8] and is expected to reduce the total installation time involved in
19 commissioning a farm, making the offshore wind market more competitive.

20 Although the continuous increase in the size of the turbines is an efficient and economical choice
21 from an operational perspective, it poses challenges and risks during the assembly and installation
22 phases. The components of wind turbines, particularly the blades and nacelle, are extremely sensi-
23 tive and require high precision during transportation and installation in the offshore environment
24 [2, 9, 10]. This high accuracy requirement makes the installation phase even more challenging with
25 larger blades, power electronics and gearbox in nacelle [11]. In current practice, various methods
26 for the assembly and installation of the turbines exist, among which the split-type installation
27 method is the most popular for installing monopile-type offshore wind turbines [12]. Under this
28 method, all the components of the turbines are individually lifted and assembled offshore, thus

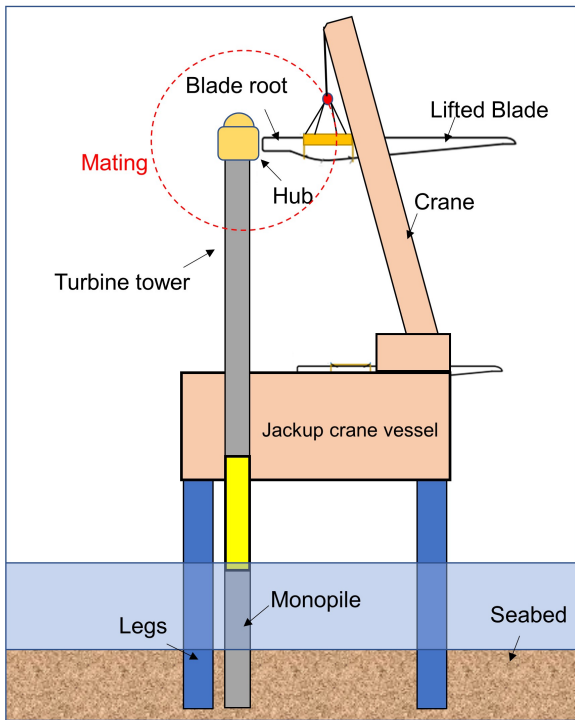


Figure 1: Mating phase of the blade installation



Figure 2: Image of a wind turbine blade being prepared to mate with hub of a turbine (source: [13])

29 enabling the lifting operation to be performed with a crane that has less lift capacity. Addition-
 30 ally, higher deck usage is utilised during the transportation phase with individual unassembled
 31 components stacked on the vessel, thereby significantly reducing the overall transportation time.
 32 All these factors make the split-type installation method highly preferred. A jack-up crane vessel
 33 (Fig. 1) is often used as the installation vessel during the assembly and installation of wind turbine
 34 generator (WTG) components, which include blades, tower, nacelle, and hub [11]. These crane
 35 vessels can be utilised in shallower waters up to depths of 30 to 50 m, and they have legs that are
 36 jacked up during the installation phase with the legs anchored into the seabed [11] (Fig. 1). This
 37 makes the vessel and the object being lifted free from wave excitations to a large extent during
 38 the lifting operation, thus providing a stable platform.

39 Nevertheless, despite the stable installation system offered by jack-up crane vessels, single-
 40 blade installation on a monopile-type offshore wind turbine is still one of the most critical and
 41 challenging methods [12, 14]. Significant relative motions between the blade root and the hub
 42 manifest during their alignment phase prior to being mated together [12], and these motions pose
 43 a significant risk of impact of the blade root with the hub (Fig. 2). Recently, there have been several
 44 incidents reported in the industry that include such impacts during mating [15]. There are several

45 factors contributing to the relative motions between these components causing such impacts. Wind
46 turbine rotor blades are aerodynamically shaped wide and long structures, and during the mating
47 phase at a very high hub height, wind-induced forces produce pendulum oscillation motions at
48 the blade root. Moreover, the large motion of the hub at the tower top, primarily developed
49 because of the wave-induced loads on the monopile structures [12, 14], makes the mating process
50 even more challenging. In general, a monopile foundation structure acts as a cantilever beam with
51 one end fixed into the seabed and possesses limited structural, soil, and hydrodynamic damping
52 with an overall damping ratio in the first aft mode of approximately 1% [12]. Thus, any lifting
53 operation in a wave excitation nearing the natural period of a monopile could trigger a resonance-
54 driven high-oscillation motion in the pre-assembled hub. Moreover, the limitation of a jack-up
55 crane vessel to shelter the monopile from wave loads during the installation phase (as the legs
56 are jacked up) makes the mating process even more critical. Overall, there could be large relative
57 motions developed between the blade root and hub during the mating phase [14]. Consequently,
58 substantial impact forces are anticipated at the blade root in the case of an accidental impact and
59 could damage the blade root locally. Such accidental events on the blade root could still have very
60 high consequences on the blade's structural integrity because the root section of a blade resists the
61 maximum flapwise and edgewise moments and torques developed in the blade during its design life
62 [16]. Thus, the severity of such accidental impacts at the blade root during the mating process is a
63 question of utmost concern. Additionally, any damage to the root connection during mating would
64 require the lifted blade to be brought back onto the vessel, causing perplexity among the offshore
65 crew regarding the decision to repair, replace or continue with another trial of mating the blade
66 with the hub. A delay in the overall installation operation is therefore inevitable, causing loss of
67 favourable weather windows, and is thus crucial for investigation. The present paper focuses on
68 the impact assessment of the blade root during such accidents, and based on the type of damage
69 obtained, it discusses the consequences on the installation tasks and suggests onboard decision
70 making following the impact. This paper also briefly discusses the choice of favourable sea states
71 for performing such mating processes.

72 To the authors' knowledge, there is still no published research on the impact assessment of
73 a blade root in a scenario wherein it is being mated with the hub. This paper is expected to
74 contribute to better planning of such offshore operations and develop guidelines that could aid
75 the offshore crew in reacting to such accidental events. This would reduce the installation cost,

76 quantify the risks involved during the critical mating operation and create confidence to match
 77 the industry's demand for installing larger turbines in the future. The remainder of this paper is
 78 organised in the following manner. Section 2 describes the problem statement, possible contact
 79 scenarios and numerical approach considered for the impact assessment in this paper. Section
 80 3 describes the modelling of the installation system representing the mating operation and the
 81 environmental conditions considered for the study. Section 4 describes the structural impact
 82 modelling of the blade root with the hub along with the constitutive material model implemented
 83 for the failure estimate at the blade root. Section 5 presents the results and discusses the relative
 84 motions developed between the root and the hub, followed by the description of failure at the blade
 85 root. Section 6 concludes the paper and finally section 7 presents the limitation and future work.

86 2. Problem statement and numerical approach

87 A wind turbine blade is designed to be attached to the pitch bearing and the hub of a turbine
 88 through mechanical joints and connections at its root (Fig. 3(a)) [17, 18]. In current practice,
 89 different types of blade root connections exist for this purpose, including T-bolt-type connec-
 90 tions, flange-type connections, and carrot- or stud-type root connections [17]. Among all these
 91 connections, the T-bolt-type connection, due to its low cost, ease of manufacturing and high re-
 producibility features, is the most popular. The present study considers the T-bolt-type root

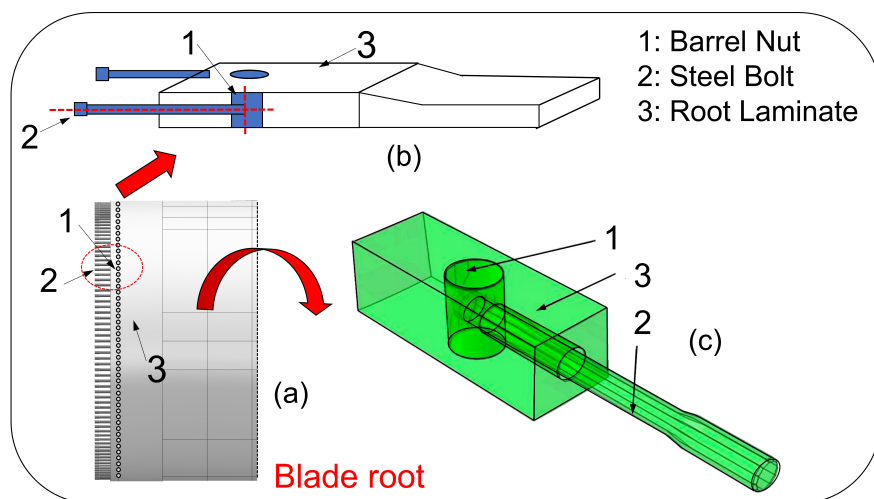


Figure 3: (a) A typical wind turbine blade root with mechanical connections (b) Zoom in view of blade root showing T-bolt connection (c) Components of a typical T-bolt connection [19]

92
 93 connection for impact investigation [20, 21, 19] (Fig. 3). These connections are uniformly spread

94 along the circumference of the blade root and are placed after the blade manufacturing process is
 95 completed. Each T-bolt connection at the blade root (Fig. 3(b), 3(c)) consists of a steel barrel
 96 nut and a steel bolt [22] fitted together into the thick composite laminate at the root. A barrel
 97 nut is a cylindrical component made of steel and is fitted into a through-the-plane hole made in
 98 the root laminate at the blade root section. The barrel nut is then joined with the surface of the
 99 laminate hole through an adhesive, and it is kept at a specific distance from the edge of the blade
 100 root [19]. The steel bolt is screwed into the barrel nut and is placed in the root through an in-plane
 101 hole drilled in the laminate (Fig. 3). The transfer of the operational loads from the blade root to
 102 the hub through these connections relies on the pre-tension of the bolt, normal stresses [18] and
 103 contact between the barrel nut and adjoining laminates.

104 In addition to these load-carrying structural connections, a few guiding connections [23] are
 105 also present at the blade root (Fig. 4). These connections are also configured in the blade as
 T-bolt connections; however, they have comparatively longer bolts, generally called ‘guide pins’

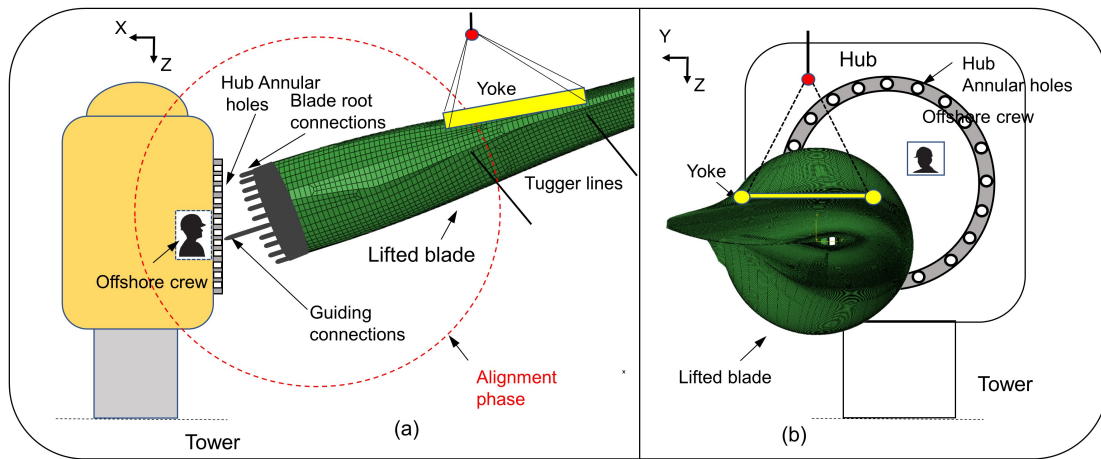


Figure 4: Guiding connection at the blade root (a) Alignment phase (b) Annular holes in the hub

106
 107 (Fig. 4). These longer bolts make it possible for an offshore banksman located inside the hub
 108 to visually monitor the blade root motion (Fig. 4(a)) with respect to the annular holes in the
 109 hub (Fig. 4(b)) and thus aid in the mating process. During the alignment phase, these guiding
 110 connections are the first to approach the hub during mating and are thus the most likely to be
 111 exposed to an accidental impact prior to other T-bolt connections at the blade root. The present
 112 paper considers a case in which a guiding connection with a guide pin at the blade root impacts
 113 the hub.

114 Moreover, it is the relative motion between the root and hub during the mating process that

115 decides the possible impact scenarios whereby a blade root impacts the hub (Fig. 5). The first
 116 impact scenario includes a head-on impact between the blade root and hub arising due to the
 117 relative motion developed along the longitudinal axis of the lifted blade (Fig. 5). This enforces
 118 impact between the hub and the guide pin bolts of the root connections in its axial direction and
 119 is likely to be less critical. This is because the bolts are designed primarily to handle axial loads
 during normal operations, and thus, an impact in this direction is expected to be less severe. The

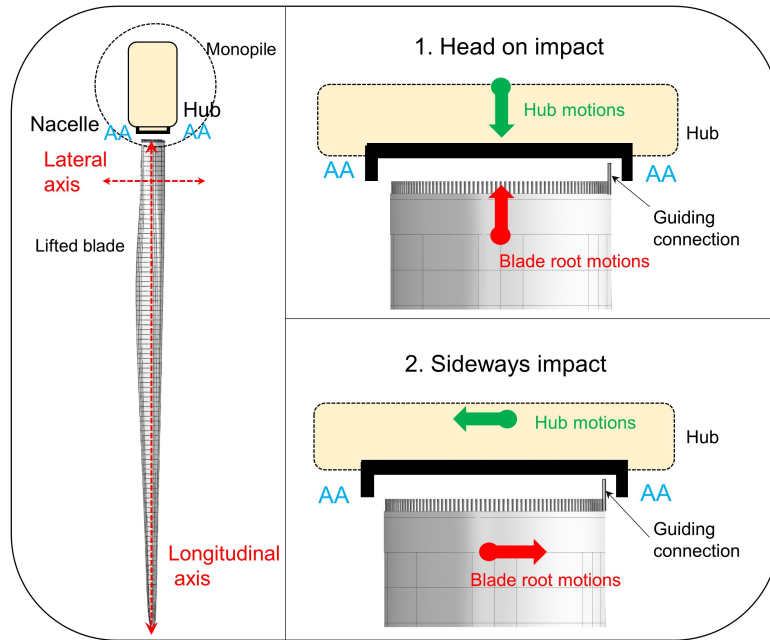


Figure 5: Impact scenarios during mating

120
 121 other impact scenario is a sideways impact between the root and hub developed due to relative
 122 motions in the lateral direction of the lifted blade (Fig. 5). This causes transverse impact forces
 123 on the guide pin bolts, which could damage the bolts and the adjoining laminate at the root
 124 connection. This is considered to be a critical scenario from a structural perspective because any
 125 damage to the composite laminates at the root is complex, cannot always be visually detected
 126 and could still severely affect the blade's ultimate and fatigue strengths [10]. The study in this
 127 paper considers the latter contact scenario for impact investigation, which will be addressed in the
 128 following sections.

129 The velocity and the forces with which the blade root impacts the hub for a particular scenario
 130 depend on their relative motions. Hence, to perform an impact assessment, it is imperative to
 131 calculate the dynamic responses in the installation system developed during an offshore mating
 132 process in a particular sea state. Thus, this study also describes the modelling of the global

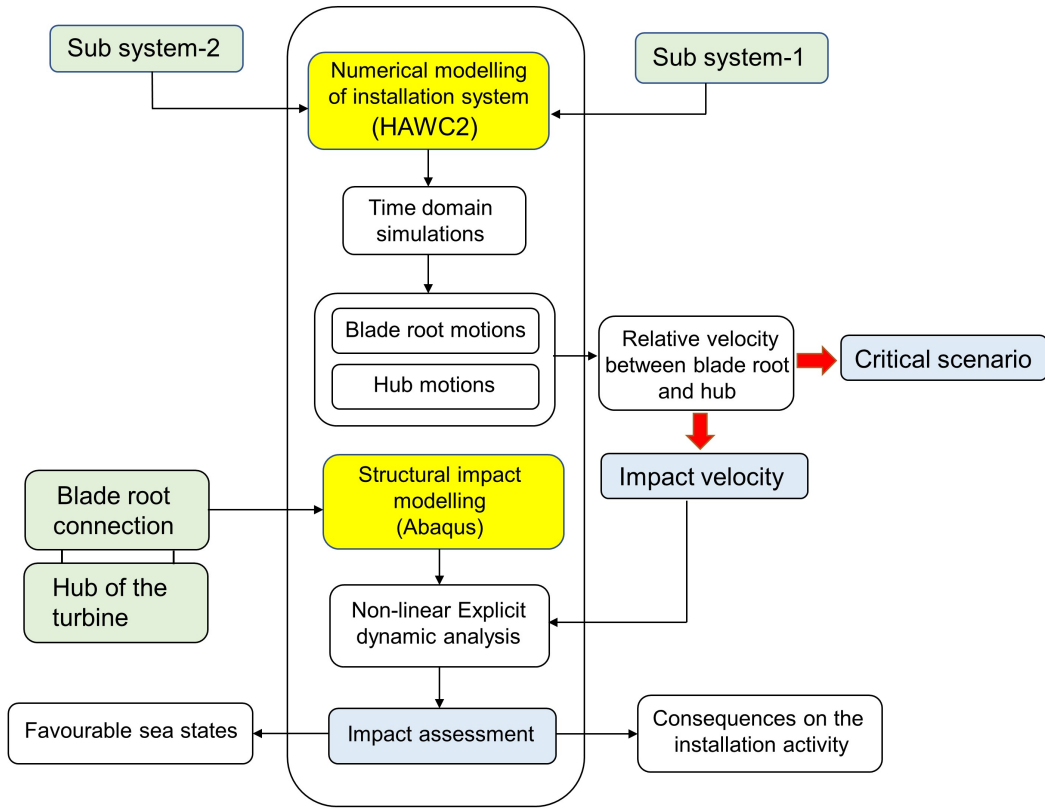


Figure 6: An overview of the numerical approach applied in the study

133 installation system describing the mating process. A complete overview of the entire approach and
 134 the analysis procedure applied in this study is presented in Fig. 6. First, the installation system
 135 representing the mating process and consisting of two sub-systems (pre-assembled monopile and
 136 single blade) is numerically modelled in HAWC2. The first sub-system (sub-system 1) accounts
 137 for the hydrodynamic and soil models for the monopile and wind drag loads on the tower, nacelle
 138 and hub while the other sub-system (sub-system 2) accounts for the aeroelasticity of the blade
 139 during lifting. Then, time-domain simulations are conducted for wave and wind conditions, and
 140 the relative velocity between the blade root and hub is analysed. Second, the blade along with
 141 the T-bolt connection at its root and the hub are modelled using the finite element method, and
 142 the impact investigation is performed using Abaqus Explicit. The modelling technique considers
 143 the three-dimensional stresses at the root connection along with a contact non-linear formulation
 144 and the entire inertia of the blade for impact investigation. Then, the damages occurring at the
 145 blade root for different impact velocities corresponding to different sea states are analysed. Finally,
 146 based on the type of damage obtained, the consequence on the installation activity after impact
 147 and discussions on the choice of a favourable sea state for mating operations are presented.

148 3. Modelling of the global installation system

149 HAWC2 was used to model the global installation system. HAWC2 is an aeroelastic code
150 developed by the Technical University of Denmark [24]. This code is based on multi-body dynamics
151 and has been widely used for dynamic response analysis of wind turbine systems in the time domain.
152 It has modelling capabilities to account for structural dynamics while considering external effects,
153 loads and control systems. The structures constituting the installation system are divided into
154 a number of independent objects in HAWC2, with each body modelled as Timoshenko beam
155 elements. The bodies are connected to each other through couplings.

156 A jack-up crane vessel, a lifting system, and a pre-assembled monopile are involved. The global
157 installation system provides a simplified representation of the physical system, which is used for
158 estimating the relative motions between the blade root and the hub. It is assumed that both the
159 jack-up vessel and crane are rigid and jack-up is rigidly fixed to the seabed with pile-soil interaction
160 for its legs ignored. In this way, the jack-up crane vessel is not explicitly modelled, and the crane
161 tip is simplified as a fixed boundary condition. This simplification is also adopted in [14, 25], as
162 proprietary information of the jack-up crane vessel is not available. The global installation system
163 includes two sub-systems (Fig. 7): (1) a pre-assembled monopile system and (2) a single-blade
164 system. These sub-systems along with their modelling details and the basis for their response
165 evaluation are discussed in the following.

166 3.1. Pre-assembled monopile system

167 The first sub-system consisted of a pre-assembled monopile foundation, a tower, a nacelle, and
168 three hubs (Fig. 7). The monopile support structure for the DTU 10 MW wind turbine utilised
169 in this study is designed by Velarde (2016) [26] and has a diameter of 9 m with a pile penetration
170 depth of 45 m. Assuming the soil properties of a uniform sand layer, Velarde [26] extracted the
171 lateral stiffness of the soil represented by p - y curves from finite element analysis. In HAWC2, the
172 monopile foundation is modelled by Timoshenko beam elements, and the soil effect is represented
173 by distributed springs, which idealises the pile as a free-free beam with lateral springs distributed
174 along the adjoining soil portions; see Fig .7. The damping ratios of the first fore-aft and side-side
175 modes of the monopile system were tuned to be approximately 1%, which is consistent with the
176 experiments on monopile foundations [27, 28]. Moreover, the tower, nacelle, and hubs used in
177 this sub-system were based on the DTU 10 MW reference wind turbine [29], and these structural

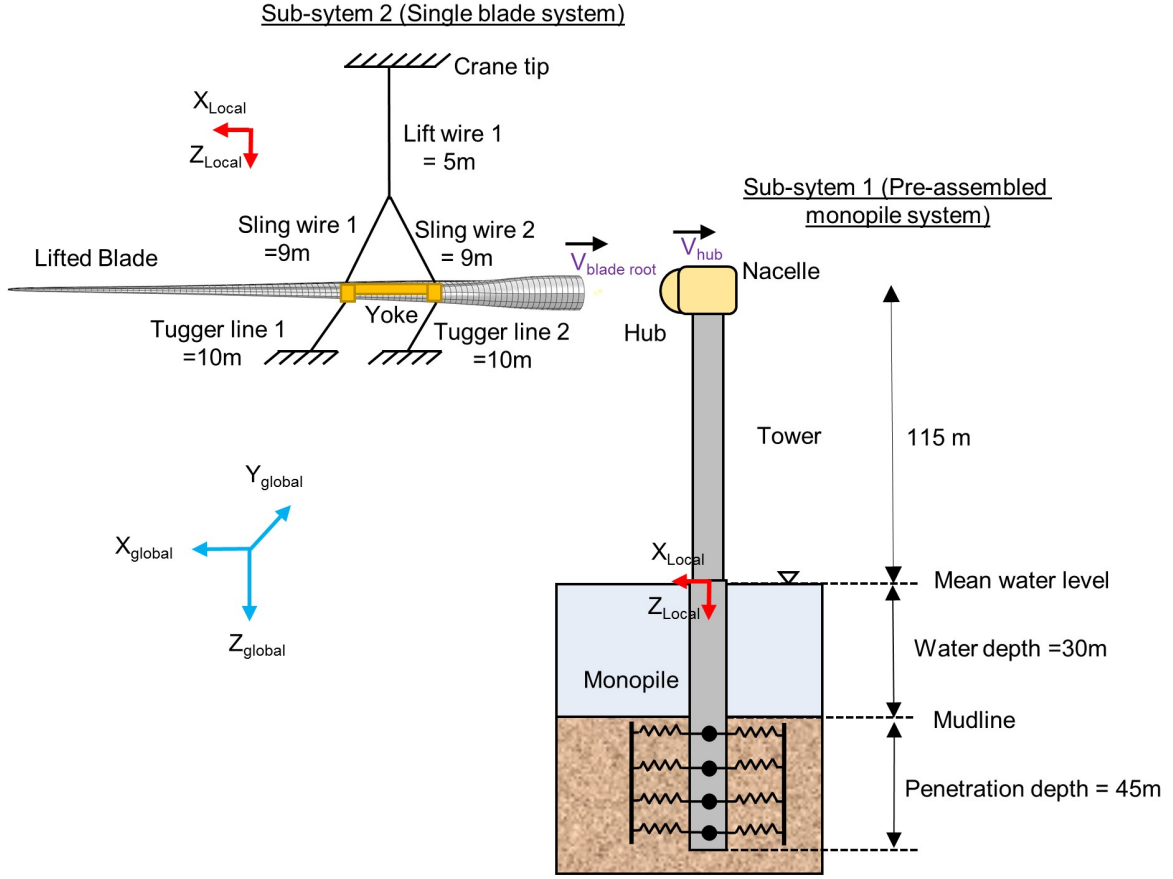


Figure 7: Modelling of the global installation system and its sub-systems

178 components were also modelled in HAWC2. The characteristics of the different components of the
 179 pre-assembled monopile system are listed in Table 1.

180 There are hydrodynamic loads acting on the monopile structure. In HAWC2, the hydrodynamic
 181 loads are evaluated by Morison's equation [30, 31], which is applicable to slender structures. The
 182 hydrodynamic force per unit length normal to each strip is expressed as:

$$f_s = \rho C_M \frac{\pi D^2}{4} \ddot{x}_w - \rho (C_M - 1) \frac{\pi D^2}{4} \ddot{\eta}_1 + \frac{1}{2} \rho C_D D (\dot{x}_w - \dot{\eta}_1) |\dot{x}_w - \dot{\eta}_1|, \quad (1)$$

183 where ρ is the density of sea water, taken as 1029 kg/m^3 ; D is the monopile diameter, taken as 9
 184 m; C_M is the mass coefficient, assumed as 2 in this study; and C_D is the drag coefficient, taken as
 185 1. Furthermore, \dot{x}_w and \ddot{x}_w are the velocity and acceleration, respectively, of water particles at the
 186 centre of the strip, and $\dot{\eta}_1$ and $\ddot{\eta}_1$ are the velocity and acceleration, respectively, of the monopile
 187 foundations. Morison's equation consists of drag and inertial terms, of which the inertial term is
 188 dominant [12, 14]. The Morison's equation is suitable for calculating hydrodynamic loads on the
 189 monopile structure when the ratio between the wave length and monopile diameter (D) is greater

190 than 5. For a ratio less than 5, potential flow theory should be used to calculate wave-induced
191 loads [32]. However, the application of potential theory will be computationally demanding in
192 time-domain simulations. For simplicity, a constant C_m of 2.0 was applied, which can be on the
193 conservative side with respect to the motions of the monopile.

194 *3.2. Single-blade system*

195 The second sub-system modelled in HAWC2 consists of an 86.4 m long DTU 10-MW blade
196 [29] lifted by a yoke and attached with two tugger lines along with lift and sling wires connected
197 to a fixed crane tip (Fig. 7). These tugger lines are generally used to constrain the blade motion
198 in the horizontal plane, with their attachment points in the model placed at an equal distance to
199 the blade's centre of gravity. Each tugger line was 10 m long, consisting of cables, each of length 1
200 m and were linked to each other by spherical joints, which further makes it possible for the tugger
201 lines to exhibit non-compressible behaviour during mating. Additionally, one end of each tugger
202 line and the lift wire were connected to the crane. The blade was modelled as one single body, and
203 the leading edge of the blade was oriented perpendicular to the direction of the wind (zero degree
204 pitch angle).

205 Furthermore, for evaluating the blade root motions due to turbulent wind field, Mann's turbu-
206 lence box [33] in HAWC2 was utilised. This turbulence box is based on Mann's turbulence model
207 and follows the isotropic turbulence in neutral atmospheric situations. The model also considers
208 the effect of non-isotropic turbulence by applying rapid distortion theory [33]. Since the lifted
209 blade is assumed to be in steady state and is non-rotating during the mating phase at the hub
210 height, steady aerodynamic lift and drag coefficients were utilised to estimate the wind loads on
211 each section of the blade. Here, the cross-flow principle [34] was utilised in the HAWC2 code,
212 which considers the wind flow to be two dimensional (2D) and neglects the component of the wind
213 in the spanwise direction of the blade.

214 *3.3. Load cases*

215 To estimate the relative motions between the blade root and hub during the mating phase and
216 to later consider a scenario in which the blade root impacts the hub, the environmental conditions
217 (EC) representing the mating operation in a relatively rough sea state were analysed. Moreover,
218 the paper considered all the load cases with collinear wind and wave conditions (Fig. 8(a)). A
219 load case (EC-I) was also considered where the mating operation was assumed to be performed in

Table 1: Characteristics of different components

S. No	Parameter	Value
1	Monopile diameter (m)	9
2	Monopile penetration (m)	45
3	Natural period of the 1st fore-aft mode (s)	4.2
4	Damping ratio of the 1st fore-aft mode	1%
5	Blade mass (ton)	41.7
6	Yoke mass (ton)	50
7	Tugger line mass per unit length (kg/m)	306
8	1st rotational mode of the blade about the global y-axis (Hz)	0.08

Table 2: Environmental conditions (wave-wind aligned)

EC	H_s (m)	T_p (s)	U_w (m/s)	TI
I	2	4	10	0.12
II	2	6	10	0.12
III	2	8	10	0.12
IV	2	10	10	0.12

220 a sea state with a wave spectral peak period (T_P) close to 4 s, which approaches the first fore-aft
 221 natural period of the monopile. This is expected to provide very high hub motions at the tower
 222 top and is critical to study (Fig. 8(a)). Additionally, the mean wind speed (U_W) considered in this
 223 paper was taken as 10 m/s at the hub height, which is regarded as an acceptable wind condition
 224 for blade installation in industry [9]. A value of 0.12 was taken as the turbulence intensity (T_I),
 225 which is for a given U_W and for a particular turbine class obtained from the IEC 61400-1 [35]
 226 guidelines. Table 2 lists all the load cases utilised in this paper, where EC in the table stands
 227 for environmental conditions, H_S stands for significant wave height, T_P stands for spectral peak
 228 period, U_W stands for mean wind speed, and T_I stands for turbulence intensity. The irregular
 229 waves in this study were generated using the JONSWAP spectrum [36]. Finally, time-domain
 230 simulations for dynamic response analyses were performed with a time step increment of 0.01 s.

231 For each case of environmental conditions listed in Table 2, five 30-min (1800 s) simulations with
232 random wave and wind seeds were performed to reduce statistical uncertainties, and the motions of
233 the blade root and the hub were obtained. Parameters such as the time step increment and number
234 of seeds for the analysis are chosen based on a sensitivity study. Further, each simulation lasted
235 2200 seconds, and the initial 400 s were discarded in the post-processing to neglect any transient
236 effects. Here, an average of five seeds for each load case, with each seed evaluated for 30-min 90%
237 fractile extreme value, was used for estimating the maximum relative velocity between the root
238 and hub. This value is utilised as the reference velocity for the impact analysis and was assumed to
239 be conservative. It was also assumed that the inertia of the monopile system is substantially larger
240 than that of the blade system and that the motion of the hub is not affected by the blade impact.
241 Hence, the relative velocity between the blade root and the hub evaluated from the HAWC2 code
242 is suitable for the impact investigation in Abaqus. This is also addressed in section 5, where the
243 displacement and acceleration of the hub motion with and without the blade impact are presented
244 and discussed.

245 **4. Structural modelling of the guiding connection at the blade root**

246 After the dynamic response analyses were performed based on the modelled installation system,
247 finite element structural modelling of the blade root connection was required to investigate the
248 consequence of its impact with the hub during mating. In this study, we consider the impact of a
249 single guiding connection at the blade root, given that these guiding connections (Fig. 9) are the
250 first to suffer impact with the hub during mating. The choice of studying the impact of a single
251 guiding connection is conservative, as this assumption implicitly neglects any load distribution to
252 the adjacent bolts during the impact event. Although it is likely that several bolts are involved
253 in the impact, this conservative approach renders the assumption most relevant according to the
254 objective of this study. A guiding connection at the blade root is principally a T-bolt connection,
255 which has a barrel nut and a longer steel bolt (guide pin) fitted into the blade root laminate
256 through in-plane and through-the-plane holes. Therefore, modelling such a connection requires
257 the development of a three-dimensional finite element model that includes all these components
258 with the implementation of a contact non-linear formulation. The modelling details are explained
259 below.

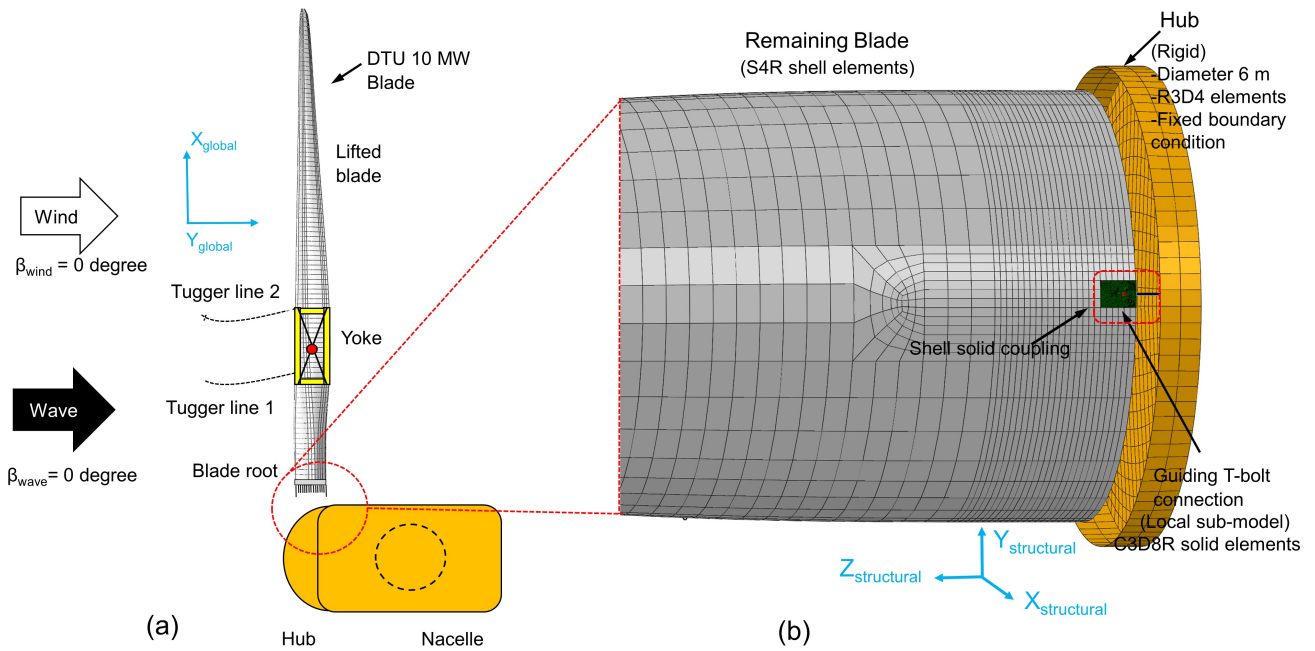


Figure 8: (a) Illustration of the environmental conditions (b) Finite element modelling of guiding connection at the blade root (rotated view with ninety degree with respect to (a))

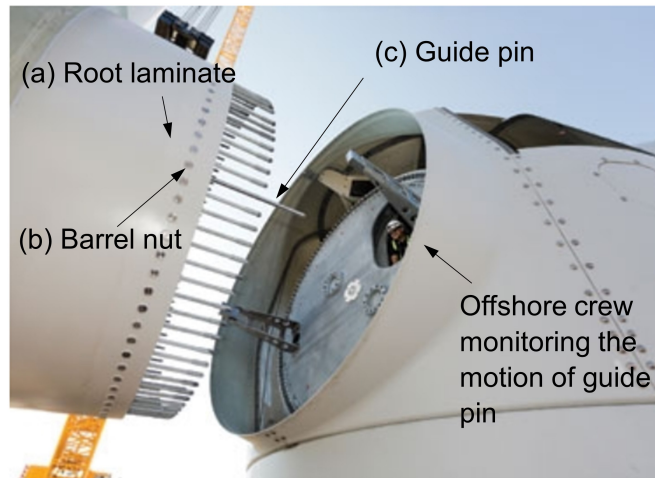


Figure 9: Components of guiding connection of the blade root observed from a real time mating operation [37]

260 *4.1. Numerical modelling method and impact formulation*

261 The three-dimensional finite element modelling and analyses in this study were performed using
 262 the Abaqus Explicit environment, a commercial finite element software developed by Dassault
 263 Systèmes Simulia Corp [38]. The explicit-based algorithm was chosen due to its capability to
 264 perform better than the implicit code while handling problems involving complex interactions, large
 265 rotations, and large deformations [39]. Hence, it was utilised for our case where we consider the

266 blade root impacting the hub, which involves complex interactions. The algorithm further utilises
267 the central difference operator and elements with a lumped mass matrix formulation [38], where the
268 kinetic state and the dynamic equilibrium are satisfied at each time increment based on the solution
269 known from the previous time increment. Nevertheless, the algorithm is conditionally stable [38],
270 requiring a time increment for stress wave propagation that is less than a minimum stable time
271 increment and is estimated automatically by the solver. However, the algorithm requires a sound
272 check of energy history after the analysis to validate the numerical model’s stability and suitability.
273 We developed the three-dimensional model of the guiding connection at the blade root and the hub
274 for impact investigation by utilising the modelling capabilities in Abaqus CAE (Computer-Aided
275 Engineering) along with its scripting interface capabilities, the specifics of which are discussed
276 below.

277 The base structural model utilised in this study was the DTU 10 MW reference wind turbine
278 blade [29], where all the information including its finite element model, material properties and
279 layup were obtained from their repository website *dtu-10mw-rwt.vindenergi.dtu.dk*. The blade is
280 86.4 m long and has a root diameter of 5.4 m, with its external and internal geometries originally
281 discretised with shell elements. The main purpose of the blade was to investigate upscaling effects
282 of blade length (from 5 MW to 10 MW) on its ultimate strength performance. Hence, the original
283 model derived from the DTU repository had no explicit connection modelled at the root or any
284 region in the blade and was defined with smeared properties. However, for the present study,
285 the guiding connection at the blade root for the DTU 10 MW blade was required and was thus
286 designed and developed separately with three-dimensional solid elements. This will be referred
287 to in this study as a ‘local sub-model’ (Fig. 8(b), Fig. 10), and the name ‘sub-model’ must not
288 be confused with the sub-modelling technique in Abaqus, where the solution of a local model is
289 derived from a global coarser model.

290 The local sub-model consisted of (1) composite root laminate (represented by green colour in
291 Figs. 10 and 11) with a thickness of 100 mm and had an in-plane hole (P) and through-the-
292 plane hole (Q), (2) steel barrel nut with a diameter (ϕ_D) of 56 mm (represented by red colour),
293 and (3) steel bolt (guide pin) with a nominal diameter (ϕ_d) of 28 mm and length (L) of 400
294 mm. The dimensions of these components of the guiding connections are based on the practice in
295 industry [19, 20], which were further validated based on a static strength design check for maximum
296 flapwise and edgewise bending moments developed at the root section of the DTU 10 MW blade

297 for extreme design loads [16, 29, 40]. In addition, the developed local sub-model was connected
 298 with the remaining structural shell model (represented by grey colour in Fig. 8(b) and Fig. 11)
 299 at its root, with a set of distributed coupling constraint equations (represented by red dots, Fig.
 11), by utilising the ‘shell to solid coupling’ method available in Abaqus [38]. This shell to solid

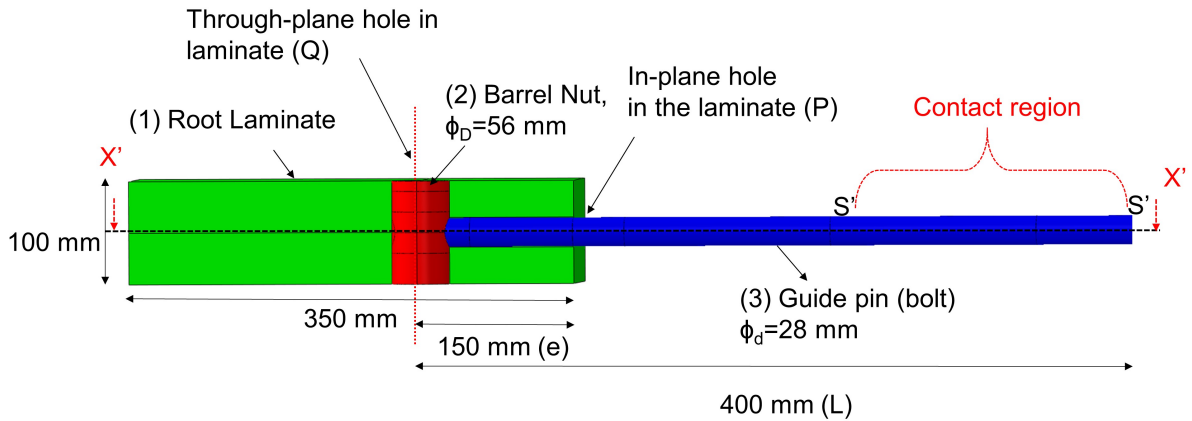


Figure 10: Dimensions and components of the local sub-model

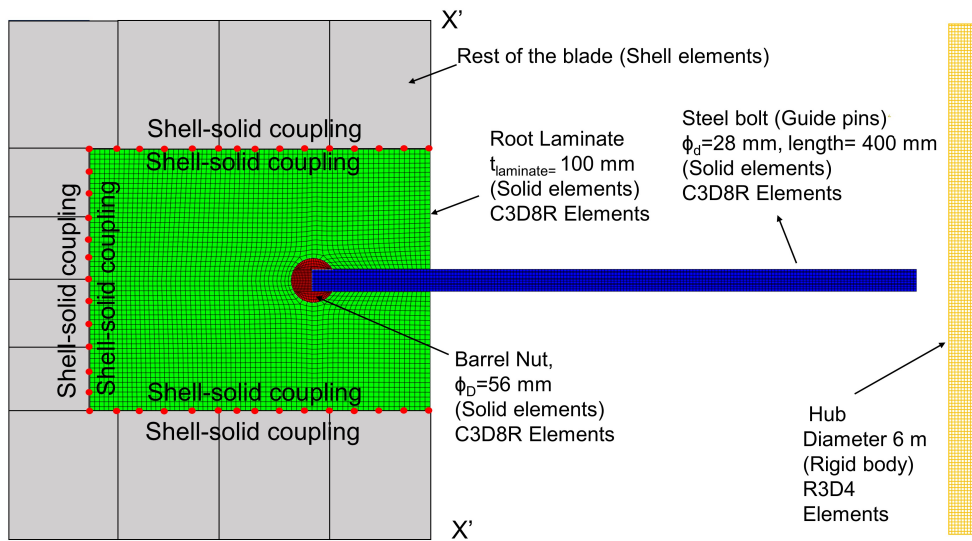


Figure 11: Shell to solid coupling of the local sub-model with the blade root (X'X')

300
 301 coupling feature enables the local detailed 3D model to be kinematically coupled to a coarser shell
 302 element region [38]. This is required to account for computational efficiency, where the analysis can
 303 be performed on elements considering three-dimensional stresses, while the entire blade discretised
 304 with coarser shell elements could provide the inertial effects to capture the true dynamics of the
 305 problem involving impact.

306 Furthermore, to model the root laminate and assign material properties to it, the information
307 of the stacking sequence of the composite plies at the root region is required. The details of
308 the layup at the blade root are generally confined to the industry's specific knowledge [40], and
309 limited information is available in the literature published to date. Moreover, the DTU 10 MW
310 blade is a non-existent blade and does not have a root-specific layup plan. The blade had shear
311 webs extended until its root with a few regions even fused with balsa, which is not characteristic
312 of a practical existing blade root used in industry. Consequently, the layup available from the
313 parent definition was not utilised in this study for modelling the laminate at the local sub-model.
314 Generally, a laminate at the root is kept conservatively thicker compared to other regions in the
315 blade and is designed with either quasi-isotropic laminates having plies oriented in a $[0/+45/-$
316 $45/90]$ layup or with a triaxial-type layup with $[0/+45/-45]$ plies [19]. In this study, the layup in
317 the form of $[0/+45/-45]$ was considered as the principal layup for the root laminate due to the
318 availability of material properties obtained from [41]. These material properties correspond to the
319 inputs from a blade manufacturer and were thus considered suitable.

320 The local sub-model at the blade root was defined with a $[0/+45/-45]$ stacking layup plan and
321 had a thickness of 100 mm. The composite laminate was modelled as a homogeneous orthotropic
322 material, with elastic mechanical properties of the laminate derived based on the homogenisation
323 principle [20, 42]. Such an approach simplifies the modelling of laminates at the root, which in
324 reality would have hundreds of layers of composite plies and would be an enormous computational
325 expense if all the layers are modelled individually with solid elements [42]. The homogenisation
326 principle is based on uniform linear displacement fields and computes the stiffness matrix of the
327 homogenised laminate as the weighted average of the individual properties of the chosen principal
328 layup. This approach enables predicting any failure state in the composites based on a maximum
329 stress failure criterion. However, any distinct failure mode in the laminate, such as matrix cracking,
330 fibre kinking or any delamination between the plies, cannot be explicitly modelled. Nevertheless,
331 the work on progressive modelling of these failure modes at the blade root due to impact is a
332 question of ongoing research and is beyond the scope of this paper. Furthermore, the threads
333 at the guide pin bolt were neglected in this study, with one end of the guide pin (head) being
334 inserted into the barrel nut and were together tie constrained. The tie constraint in Abaqus is
335 a feature that enables a rigid fixity between the barrel nut and the guide pin head without any
336 threaded connections. The guide pin head tied into the barrel nut enters through the in-plane

337 hole of the laminate. The in-plane hole had a diameter of 29 mm and was kept slightly larger
338 than the nominal diameter of the guide pin bolt as is practiced in industry and initially does
339 not have any contact with the bolt. The contact interaction was still defined between them to
340 model any possible contact during the impact event with the hub that can induce failure stresses
341 in the laminate. Again, the barrel nut was appended into the through-the-plane hole at the root
342 laminate, with contact defined under the general contact algorithm available in Abaqus Explicit
343 along with a hard contact pressure over-closure interaction and frictionless behaviour. This was
344 assumed to be suitable in this study because the adhesive that connects the barrel nut with the
345 laminate in reality has a very limited structural stiffness and is only used to keep the barrel nut
346 in position in the laminate hole [19].

347 The hub, with which the impact of the guiding connection is considered in this study, had
348 a diameter of 6 m and was modelled (represented by yellow colour, Fig. 8 (b) and Fig. 11) as
349 a rigid body with a general structural representation and was discretised with 4-node, bilinear
350 quadrilateral rigid (R3D4) elements. It was further constrained in all degrees of freedom. The
351 contact between the hub and the portion of the guide pin (S'S') considered for impact in this
352 study (Fig. 10) was defined as a part of a general contact algorithm, implemented with penalty
353 enforcement and a hard contact pressure over-closure interaction behaviour. The tangential contact
354 behaviour between the impacting surfaces were defined using the friction coefficient value of 0.3
355 and is taken from [43, 44]. The value is typical for metal to metal, and metal to plastic [45, 46]
356 contact surfaces during the impact simulation. Since the relative sliding distances between surfaces
357 involved in the contacts are small, the value of the friction coefficient is not expected to have any
358 significant influence on the analysis results. Furthermore, no other equipment involved in the
359 lifting— such as yoke, tugger lines or lifting wires— was considered in the finite element model. All
360 the nodes along the blade root section were connected with a reference node defined at the centre
361 of the root section by a kinematic coupling constraint. This constrains the motion of all the nodes
362 at the blade root with the motion of the reference node in a given degree of freedom. Finally, the
363 local sub-model had a refined area with solid brick elements of size 5.56 mm and was discretised
364 with a total of 109K C3D8R elements. The element size was chosen based on a mesh convergence
365 study, and the details will be discussed in section 5. The C3D8R elements are standard hexahedral
366 continuum solid elements with eight nodes and reduced integration. The remainder of the blade
367 was modelled with 4-node general-purpose thick shell elements (S4R elements) with interfacial

368 shell elements, which were coupled with the solid submodel having a refined mesh of size 20 mm.
369 The other regions of the blade had a coarser mesh because their major contribution in the analysis
370 was to account only for inertial loads during the impact. Finally, these analyses were performed
371 using the Abaqus/explicit algorithm, with an automatic stable time increment ranging $10e-7$ s,
372 and they were run on an HPC machine with a cluster of 2 nodes, taking approximately 34 hours
373 to complete 1 second, which is the total simulation time. Note that the impact velocity used in
374 Abaqus/explicit for damage assessment is obtained based on multi-body simulations in HAWC2,
375 where the blade is modelled with beam elements. Therefore, the global stiffness of the blade based
376 on beam and shell/solid elements were compared. The mass distributions, centre of gravity, and
377 eigen frequencies of both the blade models were compared and verified to be in close agreement.
378 This implies that these models are comparable and thus suitable for the study.

379 4.2. Implemented constitutive material model

380 4.2.1. Maximum stress criterion

381 In this study, a maximum-stress-based criterion is considered for predicting failure in the com-
382 posite laminate at the blade root. This criterion is one of the simplest and most widely utilised
383 failure models for the composite laminate [47]; however, it does not consider interactions between
384 stress components. Nevertheless, this criterion is considered appropriate for our case because the
385 focus of the study here is to estimate failure loads in the composite laminate rather than progressive
386 damage analysis of the composite. In addition, since the impact is not being considered directly
387 between the hub and the thick laminate at the root, discrete layer modelling is avoided at this level
388 of analysis. Here, the individual normal stresses in 1 (σ_{11}), 2 (σ_{22}) and 3 (σ_{33}) directions and the
389 shear stresses in 1-2 (σ_{12}), 1-3 (σ_{13}) and 2-3 (σ_{23}) planes are compared with their corresponding
390 maximum allowable strength values. The failure in the laminate is predicted when at least one
391 component of the stresses computed from the analysis (post-processed in ABAQUS [38] by S_{ij})
392 exceeds the maximum allowable strength of the laminate in that particular stress state.

393 A parameter *failure index* (F_I) is defined here in the criterion to represent the state of the
394 laminate, where a value of F_I equal to or greater than 1 implies failure in the laminate. Equation
395 (2) presents a mathematically modified form for the maximum stress criterion. The failure index
396 (F_I) is defined as the maximum value obtained from the modulus of the failure index ($|F_I(S_{ij})|$)

397 estimated for each stress state ($i = 1, 2, 3; j = 1, 2, 3$) and is expressed as:

$$F_I = \max. \begin{cases} |F_I(S_{11})|; \text{ where } F_I(S_{11}) = \left(\frac{\sigma_{11}}{X^T}\right) \text{ if } \sigma_{11} > 0 \text{ or } \left(\frac{\sigma_{11}}{X^C}\right) \text{ if } \sigma_{11} < 0 \\ |F_I(S_{22})|; \text{ where } F_I(S_{22}) = \left(\frac{\sigma_{22}}{Y^T}\right) \text{ if } \sigma_{22} > 0 \text{ or } \left(\frac{\sigma_{22}}{Y^C}\right) \text{ if } \sigma_{22} < 0 \\ |F_I(S_{33})|; \text{ where } F_I(S_{33}) = \left(\frac{\sigma_{33}}{Z^T}\right) \text{ if } \sigma_{33} > 0 \text{ or } \left(\frac{\sigma_{33}}{Z^C}\right) \text{ if } \sigma_{33} < 0 \\ |F_I(S_{12})|; \text{ where } F_I(S_{12}) = \left(\frac{\sigma_{12}}{S_{12}^t}\right) \text{ if } \sigma_{12} > 0 \text{ or } \sigma_{12} < 0 \\ |F_I(S_{13})|; \text{ where } F_I(S_{13}) = \left(\frac{\sigma_{13}}{S_{13}^t}\right) \text{ if } \sigma_{13} > 0 \text{ or } \sigma_{13} < 0 \\ |F_I(S_{23})|; \text{ where } F_I(S_{23}) = \left(\frac{\sigma_{23}}{S_{23}^t}\right) \text{ if } \sigma_{23} > 0 \text{ or } \sigma_{23} < 0 \end{cases} \quad (2)$$

398 where $F_I(S_{ij})$ is the individual failure index expressed as the normalised stress exposure factor.
 399 These exposure factors are obtained for each stress state ($i = 1, 2, 3; j = 1, 2, 3$), where stresses
 400 obtained from the analyses are normalised with their corresponding strength values. The advantage
 401 of these stress exposure factors is that they explicitly state how many times the stress levels
 402 in the laminate have exceeded their allowable stresses. Any exposure factor lying in the range
 403 ($\forall : F_I(S_{ij}) \in (-\infty, -1] \cup [+1, \infty]$) suggests failure in the laminate in a particular stress state;
 404 otherwise, ($\forall : F_I(S_{ij}) \in (-1, 1)$) suggests that the stress levels have not been exceeded. Here, any
 405 negative values correspond to compressive stress exposure factors, while positive values correspond
 406 to tensile stresses. The details of the material parameters for the homogenised laminate used in
 407 this study, including the strength of the laminate, are presented in Table 3, where the subscript
 408 ‘T’ stands for tensile and the subscript ‘C’ stands for compressive. Here, the through-the-thickness
 409 strength (Z^T and Z^C) values were not reported in the literature and were thus assumed to be equal
 410 to the strength values of the corresponding unidirectional lamina used in the homogenisation.

411 4.2.2. von Mises criterion with equivalent plastic strain

412 The material utilised for the barrel nut and the guide pin bolt is a grade 8.8 steel. A generic von
 413 Mises criterion with equivalent plastic strain indicator [38] is utilised in this study for predicting
 414 any damage in these materials due to impact. The steel is modelled with plasticity behaviour
 415 along with an isotropic hardening model [38] that is used with the von Mises yield function. With
 416 this isotropic hardening model, the yield surface (σ_0) in the stress space will evolve uniformly as
 417 plastic deformation occurs [38]. The equivalent plastic strain (ϵ^{pl}) is then obtained by integrating

Table 3: Material properties implemented for the homogenised laminate

Property	Symbol	Value	Units
Density	ρ	1864.0	Kg/m ³
Young's Modulus	$E_1; E_2; E_3$	21.69; 14.67; 12.09	GPa
Shear Modulus	$G_{12}; G_{23}; G_{13}$	9.413; 4.53; 4.53	GPa
Poisson's Ratio	$\nu_{12}; \nu_{13}; \nu_{23}$	0.478; 0.275; 0.3329	-
Longitudinal strength	$X^T; X^C$	472.06; 324.16	MPa
Transverse strength	$Y^T; Y^C$	127.1; 127.1	MPa
Through thickness strength	$Z^T; Z^C$	38.25; 114.7	MPa
Shear strength	$S^l_{12}; S^l_{13}; S^t_{23}$	99.25; 78.21; 39.51	MPa

Table 4: Material properties implemented for the steel

Property	Value	Units
Density (ρ)	7850	Kg/m ³
Young's Modulus (E)	210	GPa
Poisson's Ratio (ν)	0.3	-
Yield stress(σ_y)	640	MPa
Ultimate stress(σ_u)	800	MPa

418 the equivalent plastic strain rate ($\dot{\epsilon}^{pl}$) over the deformation history ($0 \rightarrow t$) and is expressed as:

$$\epsilon^{pl} = \int_0^t (\sqrt{(2/3)\dot{\epsilon}^{pl} : \dot{\epsilon}^{pl}}) dt, \quad (3)$$

419 This is obtained by post-processing the output variable PEEQ (plastic equivalent strain) in
420 Abaqus. The data points required for defining this isotropic model, i.e. the true stress as a function
421 of logarithmic plastic strain, were calibrated from the engineering stress-strain curve obtained from
422 the literature for the grade 8.8 steel [48]. The engineering properties and mechanical strength of
423 the steel material implemented in this work are also presented in Table 4 of this paper.

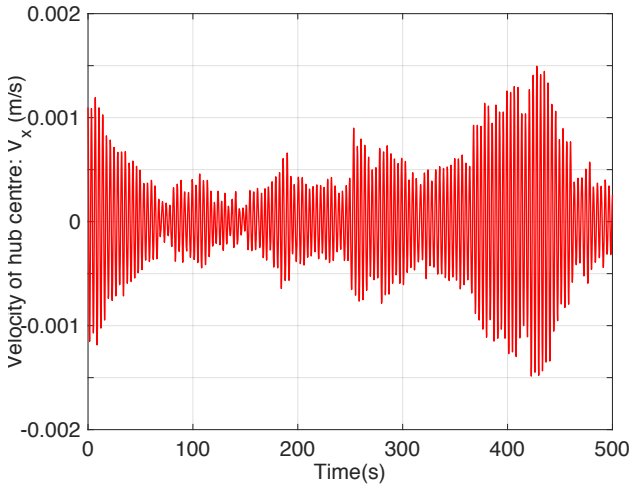
424 5. Results and discussion

425 This section presents the results and discussion on the dynamic response analyses and response
426 statistics evaluated for the installation system modelled in HAWC2. Furthermore, the results of
427 the impact investigation between the guiding connection and the hub modelled in Abaqus are
428 presented and discussed.

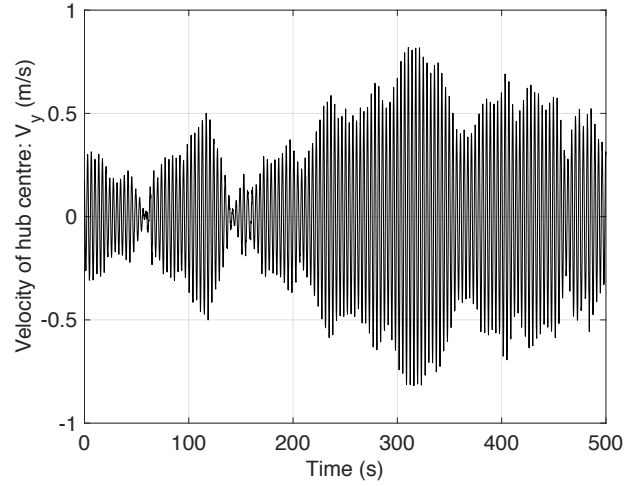
429 5.1. Hub motions

430 The responses in the hub motions depend on the hydrodynamic wave loads acting on the
431 monopile structure. Figs. 12(a)-(c) present the time histories for the velocity of the hub centre in
432 the global X, Y, and Z directions (V_x , V_y , and V_z) for the load case EC-I ($H_s=2$ m, $T_p=4$ s). These
433 figures clearly show that the motion of the hub is substantially higher in the global Y direction
434 (average of 5 seeds with 90% fractile maximum is 0.99 m/s, Fig. 12(b)) compared to its motion in
435 the X and Z directions, where the velocity is significantly low (Figs. 12(a) and 12(c); maximum
436 value of 0.0015 and 0.005 m/s, respectively). Similar observations are found for all other load cases
437 (EC-II, III, and IV) considered in this study, where the motion of the hub in the global Y direction
438 is found to be largely dominant. Consequently, this paper only considers the motion of the hub in
439 the global Y direction to calculate the relative velocity between the blade root and hub because the
440 major contribution is from the motion of the hub in this direction. The relative motion considered
441 in the global Y direction would imply that the impact scenario would involve a sideways impact of
442 the blade root with the hub, and this corresponds to the motion of the blade in the X direction of
443 the blade finite element coordinate system in Abaqus. This confirms the objective of our impact
444 assessment study, where sideways impact with the hub was critical.

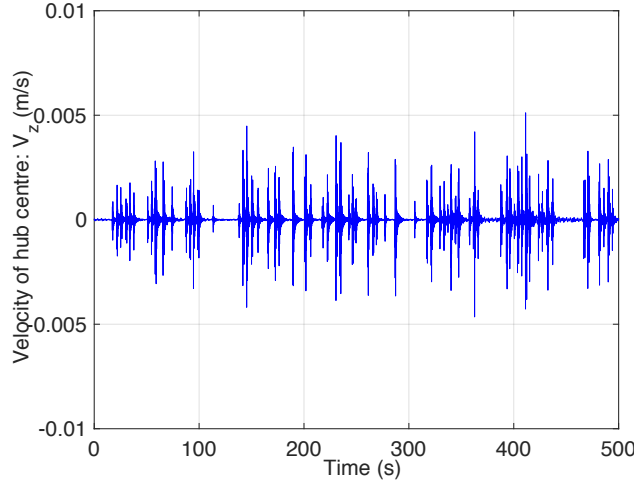
445 Fig. 13 presents the comparison between the velocity of the hub centre in the global Y direction
446 for all 4 load cases (EC-I, EC-II, EC-III, and EC-IV), i.e. with $H_s=2$ m and T_p varying as 4 s, 6 s,
447 8 s and 10 s, respectively. Load case EC-I exhibits the highest response in the hub of the turbine
448 compared to the other three load cases. This result is because EC-I has a spectral peak period (T_p)
449 of 4 s, which is near the resonance period of the monopile in its first fore-aft mode (4.2 s). Thus,
450 as a result of limited damping, it leads to a very high resonance-driven hub oscillation motion and
451 would be significantly critical for the mating process. In practice, it is very likely to have waves
452 of the same order, and thus, it would be preferable to have an artificial damping system for the
453 monopile. One way to compensate such a motion would be to apply a tuned mass damper system.
454 Such a system could prevent amplification of hub motions during such resonance actions.



(a)



(b)



(c)

Figure 12: (a) Velocity of hub centre in the global-X direction (EC-I) (b) Velocity of hub centre in the global-Y direction (EC-I) (c) Velocity of hub centre in the global-Z direction (EC-I)

455 5.2. Blade root motions and relative velocity between blade root and the hub

456 Unlike the hub motions, the blade root motions are affected by the aerodynamic wind forces
 457 and tugger line forces that constrain the blade motion. We considered a mean wind speed (U_w)
 458 of 10 m/s and corresponding turbulence intensity (T_I) of 0.12 for all the load cases considered in
 459 this study. Thus, similar response behaviour in the blade root is observed for all the load cases.
 460 Fig. 14(a) presents a comparison of the time histories for the velocities of the blade root in the
 461 global X, Y and Z directions for load case EC-I. The velocity of the blade root in the X direction

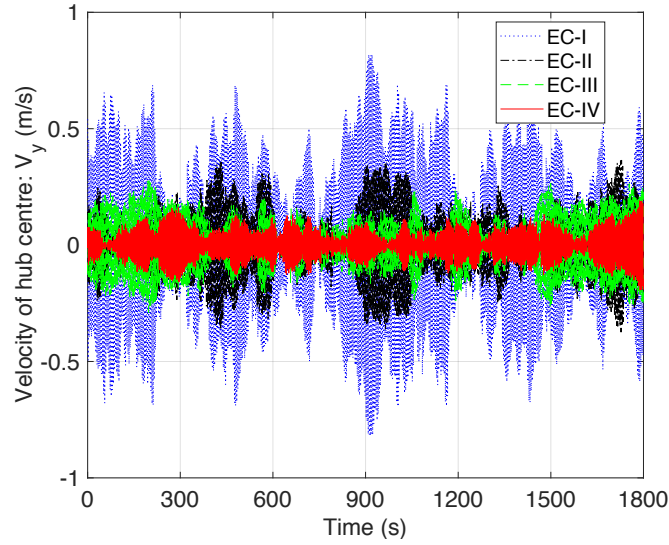


Figure 13: Comparison of hub motion for all the load cases in the global-Y direction

462 (represented by red curve) is significantly less than the velocities in the Y and Z directions. Hence,
 463 the motion of the blade in the X direction is considered to be insignificant for mating operations.
 464 Furthermore, the velocities of the blade root in the global Y and Z directions are comparable,
 465 although the former has a higher response magnitude. Nevertheless, since the hub motions as
 466 discussed are found to be insignificant in the global Z direction, this paper considers the velocity
 of the blade root in the global Y direction for evaluating the relative velocity.

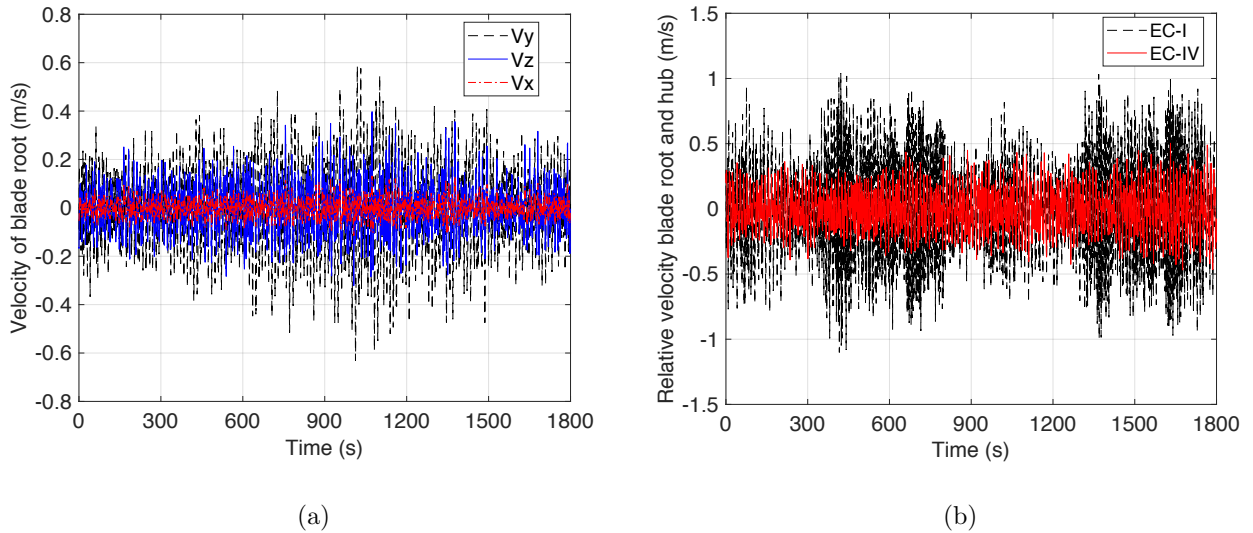


Figure 14: (a) Velocity of blade root in global X,Y and Z (EC-I) (b) Relative velocity between blade root and hub for EC-I and EC-IV

468 The relative velocities between the blade root and the hub are evaluated for all the load cases.
469 Fig. 14(b) presents the time histories for two load cases (EC-I and EC-IV), with the former
470 presenting significantly higher values due to a large contribution from the hub motion. This can
471 be confirmed from Table 5, where the magnitude of the relative velocity between the blade root
472 and hub for load case EC-I is reported to be approximately 1.3 m/s compared to EC-IV having
473 a value of 0.63 m/s. The relative velocity also decreases with increasing spectral peak period.
474 Finally, important response statistics such as mean, standard deviation (SD) and extreme value
475 (Max) for hub motions, blade root motions and the relative velocities between them are evaluated
476 based on the average of the five simulations presented in Table 5. Here, the statistical parameter
477 ‘Max’ for each load case corresponds to the average of 5 seeds, with each seed evaluated for 90%
478 fractile maximum value. The response measure ‘Max’ obtained for the relative velocity between
479 the root and hub in the global Y direction is utilized as the impact velocity for performing the
480 impact investigation in Abaqus.

Table 5: Response statistics for the load cases

EC	Velocity of hub (Y)			Velocity of root (Y)			Relative velocity (Y)		
	Mean	SD	Max	Mean	SD	Max	Mean	SD	Max
EC-I	0.92	0.01	0.99	0.53	0.05	0.59	1.18	0.11	1.30
EC-II	0.54	0.04	0.60	0.56	0.05	0.61	0.83	0.11	0.92
EC-III	0.37	0.04	0.41	0.54	0.06	0.61	0.67	0.07	0.81
EC-IV	0.2	0.02	0.22	0.53	0.05	0.59	0.49	0.06	0.63

481 5.3. Impact-induced damage assessment at the blade root guiding connection

482 The impact analyses were considered for a scenario in which the blade root guiding connection
483 during mating suffers sideways impact with the hub. Before the results of the damage assessment
484 on the blade root are presented, the validity of the numerical model’s suitability needs to be
485 discussed. Hence, a mesh convergence study for different element sizes considered for the local
486 sub-model and a discussion of the energy output history are presented and discussed first. Since
487 it is assumed in this study that the motion of the hub does not change due to impact with the
488 blade, the displacement and acceleration of the hub with and without the blade impact are also
489 presented. This result would confirm the assumption of utilising the relative velocity between the

490 blade root and hub for the impact investigation. Then, the damages occurring at the blade root
 491 guiding connection and its components are presented and discussed.

492 5.3.1. Mesh convergence analysis and energy output examination

493 A mesh convergence study is performed for the components of the guiding connection, where
 494 the consistency of the results with the element sizes used in the local sub-model is investigated.
 495 Here, the results are presented for a load case with an impact velocity of 0.81 m/s [EC-III]. The
 496 (1) maximum equivalent plastic strain (ϵ_{pl} , represented by PEEQ) developed in the guide pin,
 497 (2) through-the-thickness normal strain (ϵ_{33} , represented by LE33) developed around the in-plane
 498 hole of the root laminate, and (3) computational time normalised with 3 days of cluster time on a
 499 supercomputer are chosen as the controlling parameters. In the convergence analysis, the sizes of
 500 the C3D8R brick elements in the bolt and around the in-plane hole of the root laminate are taken
 501 as 2.49 mm, 5.56 mm, 8.16 mm and 10.28 mm. Fig. 15(a) shows a comparison of these controlling
 parameters with varying element sizes, where it can be observed that the element sizes of 5.56 mm

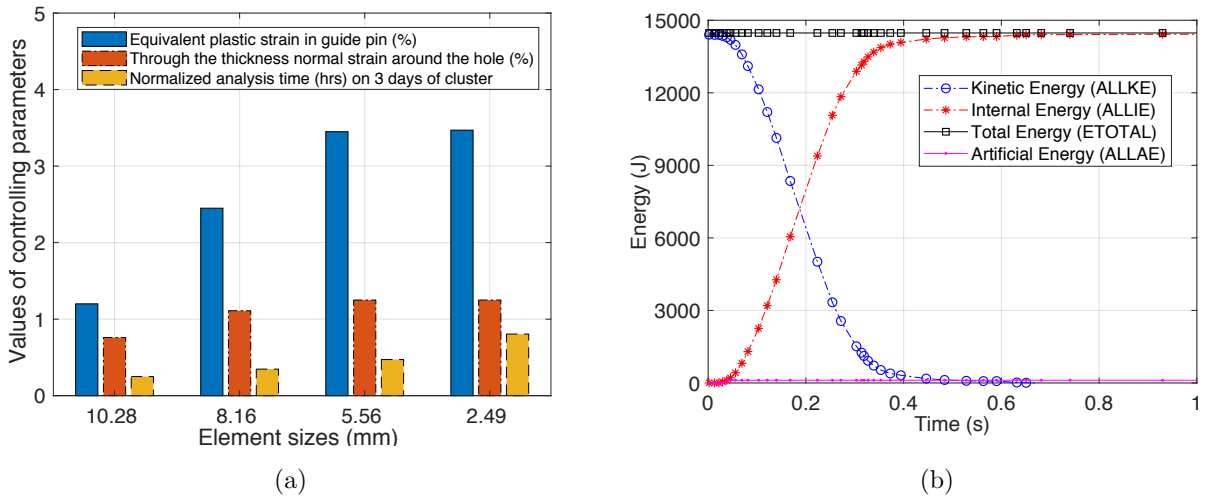


Figure 15: (a) Mesh convergence study ($V_x = 0.81$ m/s) (b) Energy evolution history ($V_x = 0.81$ m/s)

502
 503 and 2.49 mm provide consistent results for both components of the sub-model, with the former
 504 taking an analysis time that is 1.8 times faster to solve the numerical problem. Thus, the element
 505 size of 5.56 mm is chosen for discretising the sub-model and performing the impact investigation.

506 After the mesh convergence study, the energy output history results are also examined to
 507 validate the model's suitability. This is required especially for a numerical analysis based on an
 508 explicit-algorithm-based solver. Fig. 15(b) presents the energy evolution history for a case where

509 the blade root guiding connection impacts the hub with an impact velocity of 0.81 m/s. As shown,
 510 the total energy in the system (ETOTAL) is constant throughout the simulation time, with the
 511 sum of kinetic energy (ALLKE) and internal energy (ALLIE) corresponding to the total energy
 (ETOTAL). This result confirms that the energy conservation principle was satisfied for the impact

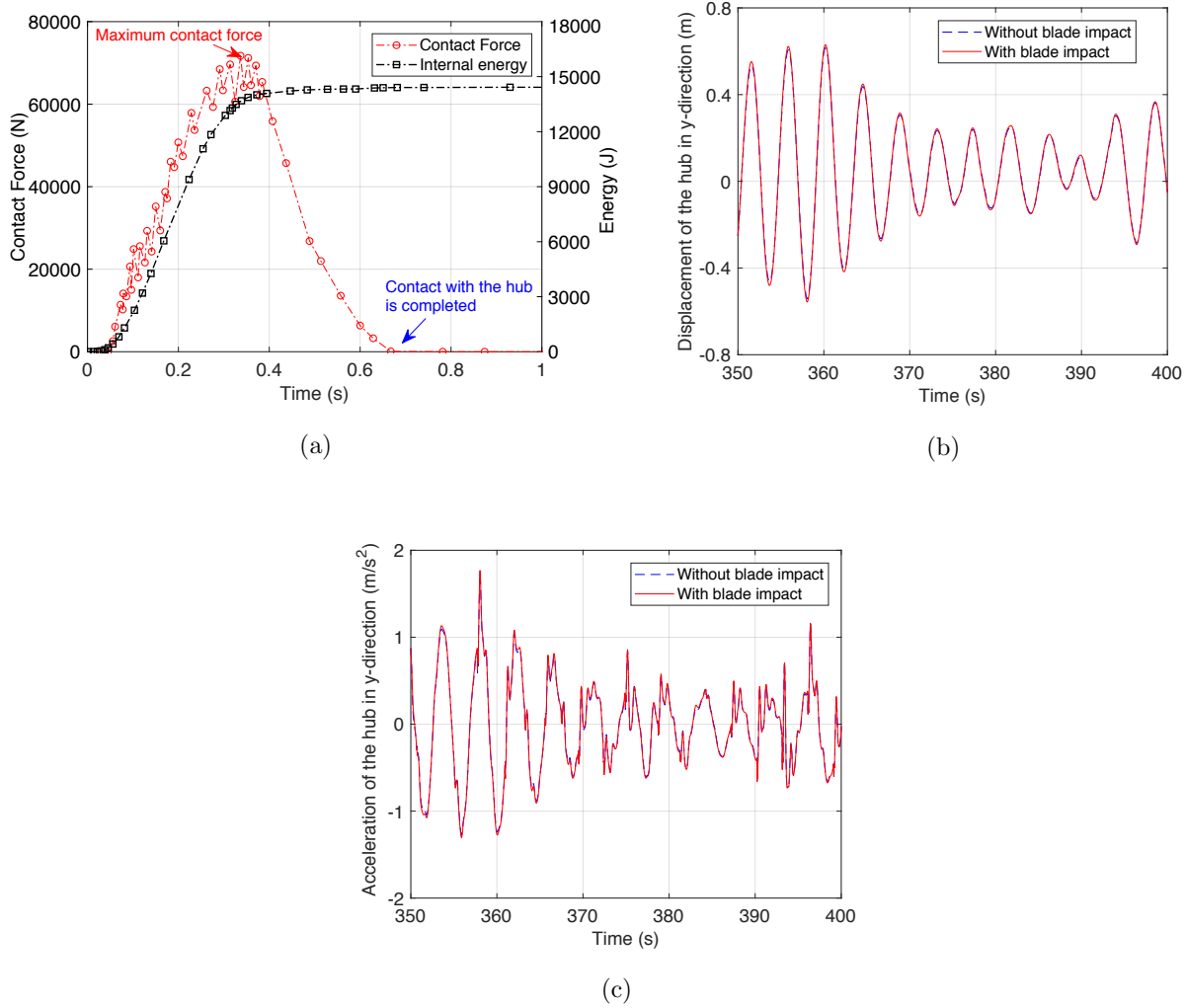


Figure 16: ((a) Contact force history with internal energy evolution (b) Displacement of the hub (c) Acceleration of the hub

512
 513 analysis. Furthermore, the artificial strain energy (ALLAE), which is developed in the numerical
 514 analysis to constrain any potential hourglass effects, is found to be significantly small (Fig. 15(b))
 515 (and was less than 2% of the total energy). Overall, these checks validate the numerical suitability
 516 of the model utilized in this study.

517 *5.3.2. Contact force history and motion of the hub with and without the blade impact*

518 Fig. 16(a) presents the evolution of the contact-force history along with the evolution of
519 the internal energy developed in the blade due to impact with the hub. It is observed that the
520 internal energy developed in the blade closely follows the contact force history curve. It can also
521 be observed from the contact force curve that the blade root guide pin comes into contact with
522 the hub at approximately 0.04 s of the simulation time, with a maximum contact force of 73 kN
523 developed at almost 0.4 s of the simulation time. This is the maximum time duration where any
524 damage in the blade due to impact is observed. The contact duration from 0.4 s to 0.63 s presents
525 a phase where the blade, due to the eccentricity of its impact, rotates as a rigid body while being
526 in contact with the hub. Finally, the contact of the guide pin with hub lasts until 0.63 s of the
527 simulation time, and the blade separates from the hub. This contact force history is then taken as
528 an input to an external force DLL (dynamic link library) in HAWC2. This is to check the blade
529 impact on the overall hub motion.

530 Figs. 16(b) and (c) compare the displacement and acceleration in the hub with and without
531 the blade impact. As shown, the effect of the blade impact on the motion of the hub is very small.
532 This result is expected because the mass of the hub is almost 10 times the mass of the blade, and
533 the compliance of the guide pin does not influence the global behaviour of the hub. This confirms
534 our assumption about the use of the relative velocity between the blade root and hub for impact
535 investigation.

536 *5.3.3. Damage assessment of the blade root and its consequence on installation tasks*

537 Fig. 17 presents the initial ($t=0$ s) and final deformation states ($t=1$ s) of the blade root (shown
538 in grey colour) for a case where its guide pin (shown in blue colour) impacts the hub (illustrated by
539 green colour) with an impact velocity of 1.30 m/s [EC-I]. As shown, due to the impact, there is a
540 permanent deformation and bending of the guide pin bolt (Fig. 17). This can be further confirmed
541 from Fig. 18, where the final strain state of the local sub-model consisting of root laminate, guide
542 pin and barrel nut is magnified and presented. It can clearly be observed that there is a substantial
543 development of plastic strain (PEEQ) in the guide pin, closer to the region where it meets the root
544 laminate and the barrel nut. This leads to significant plastic deformation in the guide pin and is
545 characterised by the pin bolt being permanently bent to an angle of approximately 15° (Fig. 18)
546 from the initial state. From an installation perspective, this bending of the guide pin bolt would
547 mean that in cases of an accidental impact during mating, the lifted blade would not be mated

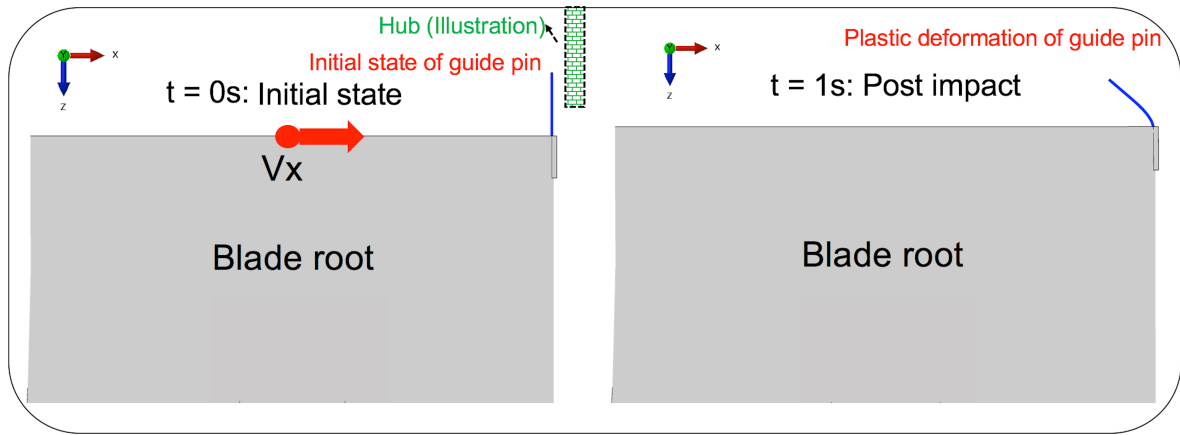


Figure 17: Pre and post impact deformation state of the blade root connection ($V_x = 1.30$ m/s)

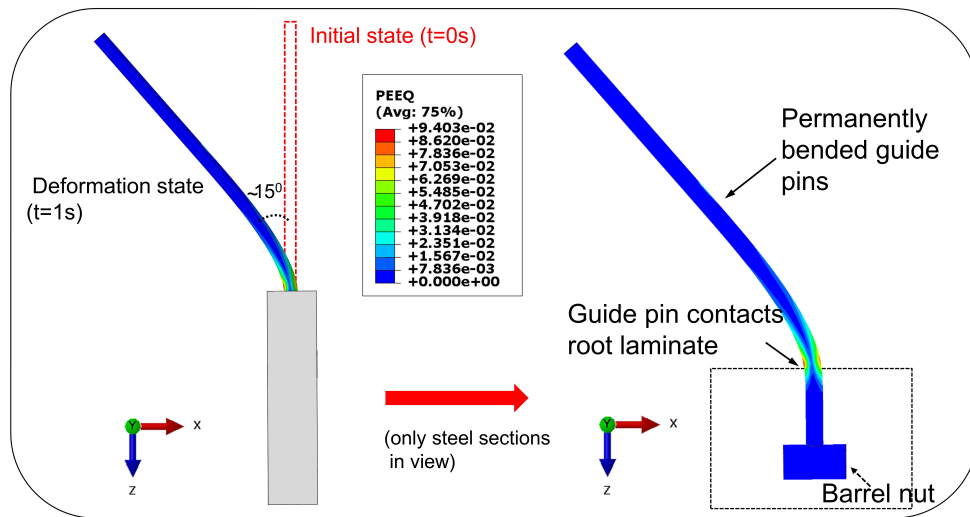


Figure 18: Plastic deformation and bending of guide pins due to impact ($V_x = 1.30$ m/s)

548 and would require being hoisted back onto the deck of the vessel with this damaged guide pin
 549 bolt requiring replacement. This would indeed lead to installation delays and increase the overall
 550 installation cost. Nevertheless, the bending of the guide pin exclusively is not considered as a
 551 critical failure mode for the blade's structural integrity because these bolts can still be replaced
 552 with newer ones and the blade is considered again for another mating trial. Additionally, as a
 553 result of such an impact, no plastic strain develops in the barrel nut, inferring a sound barrel nut
 554 before and after the impact. This is a good indicator from an installation perspective as the barrel
 555 nut is permanently attached in the blade root by an adhesive connection and, in the case of any
 556 damage, cannot be replaced with a newer one.

557 Furthermore, due to bending of the guide pin bolt during and after the impact, an impact

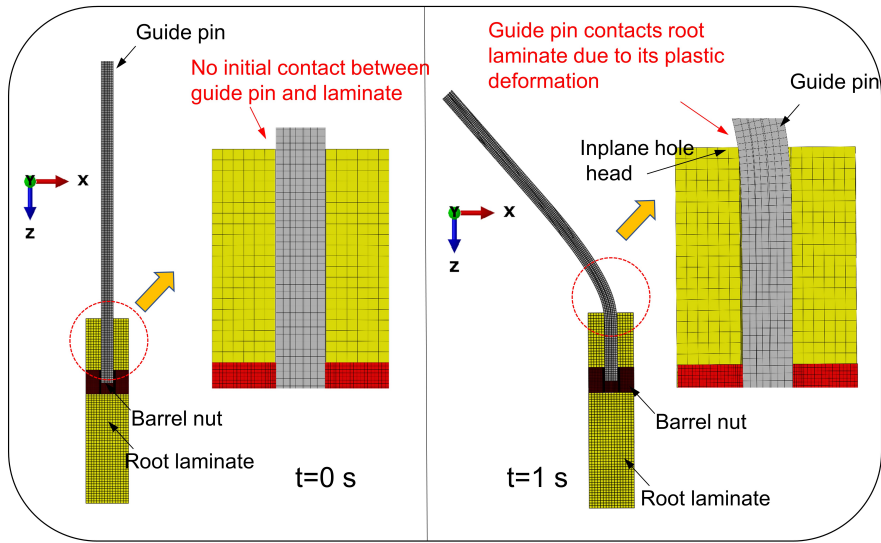


Figure 19: Contact of the guide pin with the laminate

558 occurs between the guide pin and the root laminate around the in-plane hole, which could possibly
 559 damage the adjoining laminates. Fig. 19 shows the cross-sectional cut view of the sub-model,
 560 where at $t=0$ s (initial state), it can be observed that there is no contact between the guide pin
 561 and the laminate initially. This is because in the finite element model of the guiding connection,
 562 the nominal diameter of the guide pin was kept smaller than the in-plane hole diameter at the root
 563 laminate. However, at $t=1$ s, as a result of the bending of the guide pin, contact between them
 564 could clearly be observed around the head region of the in-plane hole (Fig. 19). Since the contact
 565 interaction properties were already defined between these components in the finite element model,
 566 any possible failure occurring in the laminate due to such impact forces could be predicted based
 567 on the stress criterion implemented and are hence discussed here.

568 The impact-induced stresses developed in the laminate around the in-plane hole are investi-
 569 gated, and the failure index with normalised stress exposure factors for all the stress states are
 570 analysed. First, the in-plane stress states in the laminate are checked with their allowable values.
 571 It is found that the in-plane normal (σ_{11} and σ_{22}) and in-plane shear stresses (σ_{12}) are below their
 572 allowable values, implying that their normalised exposure factors in the laminate are below the
 573 failure threshold values. However, the through-the-thickness transverse normal stress (σ_{33}) and
 574 inter-laminar shear stresses (σ_{13} , σ_{23}) in the laminate are found to be critical and thus further
 575 reported and discussed here. This observation is consistent with the behaviour of the composite
 576 laminates whose strength in the transverse direction is significantly lower than the strength and

577 stiffness in its in-plane direction.

578 Fig. 20 presents the impact-induced stress exposure factors for the through-the-thickness nor-
 579 mal (σ_{33}) and inter-laminar shear stresses (σ_{13} and σ_{23}) developed in the laminate around the in-
 580 plane hole. These exposure factors are denoted by the parameter failure index (F_I) defined for the
 581 corresponding stress state as $F_I(S_{33})$, $F_I(S_{13})$ and $F_I(S_{23})$. Here, any exposure factor lying between
 582 1 and -1 ($-1 < F_I(S_{ij}) < +1$) suggests that the stresses in the region of the laminate lie below the
 allowable stresses (i, j) and thus have not failed. This range of exposure factors ($\forall : F_I \in (-1, 1)$)

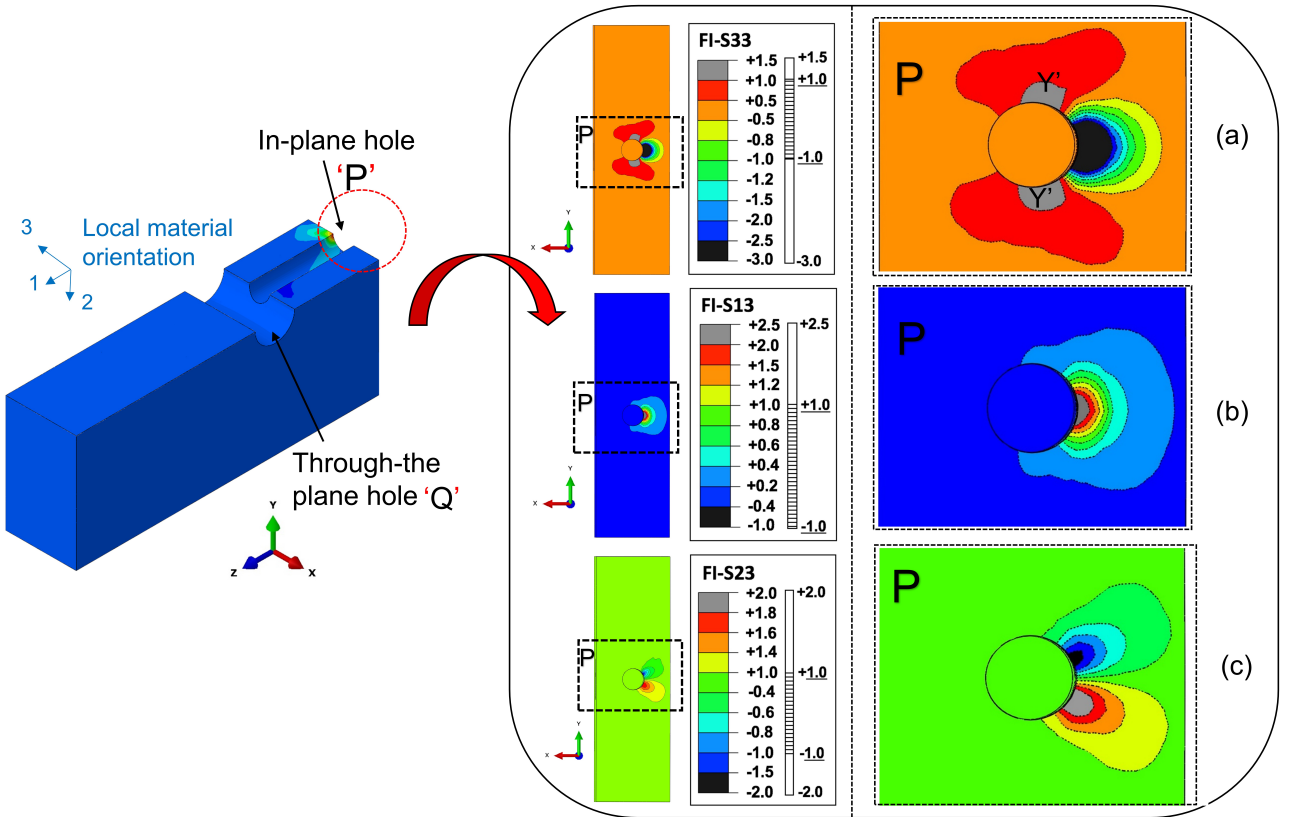


Figure 20: Failure Index representing stress exposure factors for S33, S13 and S23 (EC-I)

583
 584 is also explicitly marked with hashed lines in the legends of the contour plot in Fig. 20 for clarity.
 585 Again, any region with exposure factors lying outside this range ($\forall : F_I(S_{ij}) \in (-\infty, -1] \cup [+1, \infty]$)
 586 predicts the occurrence of failure in the laminate. As shown in Fig. 20, the regions around the
 587 in-plane hole of the root laminate have exposure factors greater than 1 in all three stress states
 588 ($\sigma_{33}, \sigma_{13}, \sigma_{23}$), implying failure in the laminate. Moreover, an exposure factor of +1.5 in $F_I(S_{33})$
 589 (Fig. 20(a)), which corresponds to tensile through-the-thickness normal stresses (shown in grey
 590 colour), developed in the transverse direction of the in-plane hole ($Y'Y'$) is a very critical failure
 591 stress state. This is due to the orientation of the plies, which are stacked in the transverse direction

592 in these regions and are highly likely to lead to delamination cracks in the Mode I crack-opening
 593 fracture mode. These delamination cracks could negatively affect the blade's structural integrity
 594 because these in-plane holes are subjected to compressive stresses during the normal operational
 595 loads. This could lead to crack growth in these regions if the damage levels are not analysed due
 596 to such impacts and the crew decides to install the blades onto the hub. Thus, in the case of such
 597 damages, it would require major repair works at the root when the blade is brought back onto
 598 the vessel. There is also a high probability that the blade had developed critical damages and is
 599 declared to be unfit from a structural perspective and hence rejected. This would lead to failure of
 600 the blade installation process, leading to heavy losses. Thus, such a failure mode is not acceptable
 601 from the perspective of the blade's structural integrity, and any environmental load case causing
 602 such damage at the root laminate in the mating phase must be avoided. Nevertheless, the extent
 603 of cracks and a fracture-mechanics-based delamination approach would require further investiga-
 604 tion and will be considered in future work. However, based on the criterion implemented for the
 laminate, this study suggests that for load case EC-I, the laminate has failed.

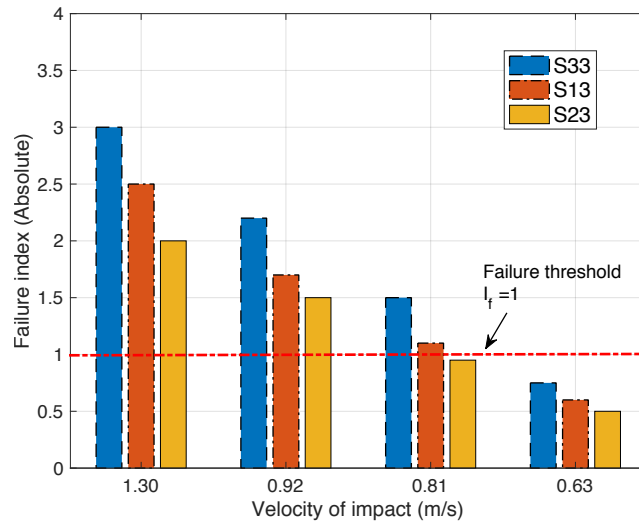


Figure 21: Failure index in the root laminate for all the load cases

605
 606 Fig. 21 summarises the failure index evaluated for the through-the-thickness normal and trans-
 607 verse shear stresses developed at the root laminate for all the load cases considered in this paper.
 608 It can clearly be observed that for all the load cases, except for EC-IV, the laminates have a
 609 failure index exceeding 1, suggesting failure in the laminates. This would mean that the mating
 610 operations of the blade root with the hub must be avoided in such sea states [Cases I, II, and III] as

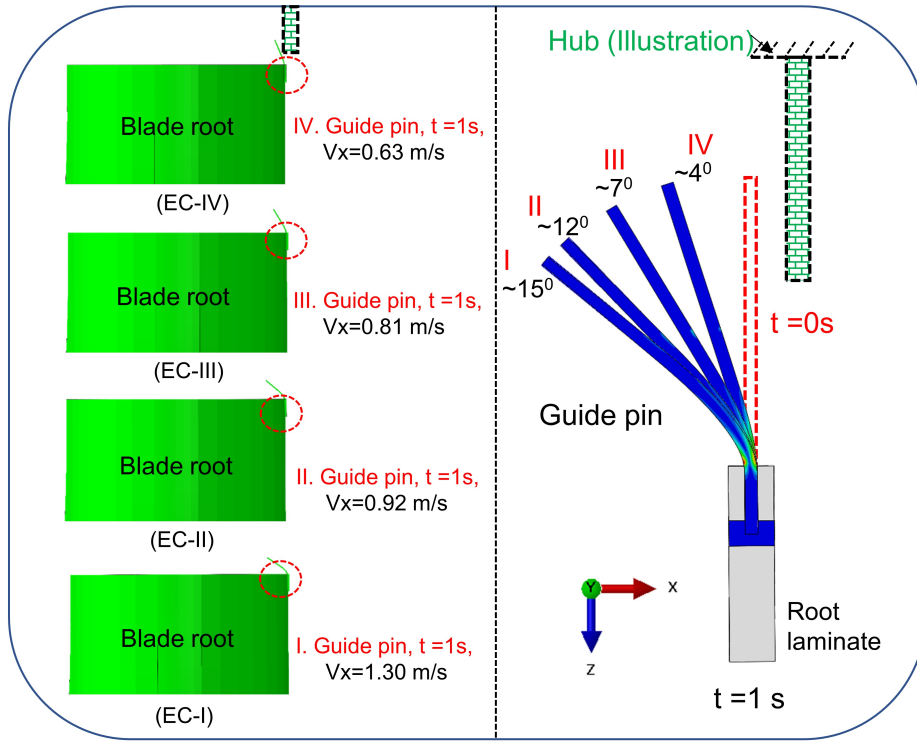


Figure 22: Plastic deformation in the guide pin for all the load cases

611 there could be high consequences on the blade's structural integrity upon its impact, given failure
 612 predicted in the laminates. Additionally, for all the load cases considered in this paper, the guide
 613 pin bolt suffers permanent deformation and bends (Fig. 22). Thus, the blade would be required
 614 to be hoisted back onto the vessel deck for all the cases, and the guide pin would be required to
 615 be replaced with a newer one. However, for load case EC-IV, since the guide pin had bent at an
 616 angle of 4° and there were no damages in the laminates, the blade can be lifted again, and another
 617 mating trial can be performed as soon as the newer bolts are reinstated.

618 5.3.4. Summary of the damages and the consequence on the installation activities

619 Table 6 illustrates the damages, post-impact consequences and planning chart for the mating
 620 operation between the blade and the hub considering impact risks. It can be observed that for
 621 all the cases due to guide pins becoming damaged, the blade would need to be brought back onto
 622 the vessel and would require repair of the blade root by replacing the damaged guide pin with a
 623 newer one. However, it is only for load case EC-IV could the blade be lifted for another trial after
 624 the replacement of guide pins with newer bolts. For the other load cases, since there is damage of
 625 the root laminate, which could develop delamination cracks, it would require further investigation

Table 6: Damage, post-impact consequences and planning chart

EC	Damages in the guiding connection			Post-impact consequences and crew decision				Planning
Variables	Guide Pin	Barrel Nut	Root laminate	Blade back on vessel	Repair	Another Trial	Further check	Sea States
EC I	D	ND	D	Y	Y	NP	R	NA
EC II	D	ND	D	Y	Y	NP	R	NA
EC III	D	ND	D	Y	Y	NP	R	NA
EC IV	D	ND	ND	Y	Y	P	NR	A

Keywords: **D**-Damaged; **ND**-Not Damaged; **Y**-Yes; **N**-No; **NP**-Not possible; **P**-Possible; **R**-Required; **NR**- Not Required; **NA**-Not acceptable; **A**-Acceptable

626 and checks on the vessel before the blade is either given another mating trial, repaired or rejected.
627 In either case, it would lead to severe installation delays and critical structural damages, and
628 it is thus preferable to accept only EC-IV as an acceptable sea state out of all the sea states
629 considered in this study. Such an approach with damage, consequences and planning chart could
630 be utilised in the future to elaborately consider the impact risks for all possible sea states and
631 evaluate response-based operational limits considering structural damage criteria.

632 6. Concluding remarks

633 This study addresses the final stage of the mating process of the blade root with the hub, which
634 is highly challenging and requires high precision. It is discussed that due to the relative motions
635 manifested during the alignment phase, an impact could occur between the blade root and the hub
636 when the guiding connection is being positioned. Here, the sideways impact of a guiding connection
637 at the blade root with the hub is investigated. For this purpose, the global installation system
638 representing the mating operation is modelled in the HAWC2 code. Four different environmental
639 load cases are considered, which represented the mating operation in a relatively rough sea state
640 and with collinear wind and wave conditions. Dynamic response analyses for all the load cases
641 are performed, and response statistics including impact velocities are evaluated. The guiding
642 connection, as a local sub-model for the DTU 10 MW blade, is separately modelled using finite

643 element modelling in Abaqus and is coupled with the blade at its root with shell solid coupling
644 feature. Finally, the impact analyses are considered with the hub for four different impact velocities,
645 each corresponding to a specific environmental load case. The major conclusions from the study
646 are as follows:

647 • The blade root motions and the hub motions during the mating phase are critical, with
648 the dominant contribution to the relative velocity coming from the latter. The hub motions are
649 quite sensitive to the spectral peak period of the waves. The maximum responses in the hub are
650 obtained for the load case for the sea state with $T_p = 4$ s [EC-I]. This approaches the natural period
651 of the monopile in the first aft mode, and it contributes to the highest relative velocity manifested
652 between the blade root and hub.

653 • The relative motion evaluated for collinear wave and wind conditions inferred the occurrence
654 of a sideways impact of the blade root with the hub as the critical impact event. From a struc-
655 tural perspective, this scenario is susceptible to large damages given the impact in the transverse
656 direction of the bolt connections.

657 • The guiding connection is modelled in Abaqus, and the root laminate is defined with a
658 homogenised triaxial layup of [0/+45/-45], with properties derived based on the homogenisation
659 principle. This study considers the finite element analysis based on an explicit algorithm. The
660 von Mises with isotropic hardening model and equivalent plastic strain criterion are utilised for
661 predicting any failure in the steel bolt, whereas a maximum stress criterion is considered for
662 predicting any failure in the composite root laminate. Failure indices are also formulated in
663 the maximum stress criterion, which present normalised exposure factors for the stress states.
664 Numerical validity based on the mesh convergence study and energy output history examination
665 for the explicit-based finite element analysis are checked, and the numerical models utilised for the
666 impact investigation are found to be suitable.

667 • It is further found that due to impact, for all the load cases, there are severe bending and
668 plastic deformations of the guide pin. Consequently, this causes the contact of the guide pin
669 with the laminate near its in-plane hole. The stresses around the in-plane hole are checked. The
670 through-the-thickness normal stresses and transverse shear stresses for all the load cases, except
671 for EC-IV, exceeded their allowable values, which suggests failure in the laminates.

672 • For all the load cases and damages in the components, consequences to the overall installation
673 task and crew decisions to repair, replace or continue with another mating trial are discussed. It

674 is noted that any damage to the guide pin bolts (a damage mode that was obtained for all the
675 load cases) would require the blade to be hoisted back onto the vessel and would cause installation
676 delays. However, a case with only guide pins being damaged is not a critical failure mode, as
677 these can be replaced with newer ones and the blade could be lifted for another mating trial.
678 It is further discussed that any damage to the laminates during such impact could lead to the
679 progression of delamination cracks in Mode I crack-opening fracture mode and would be critical
680 for the blade's structural integrity, requiring a further check. Thus, if such damage modes occur,
681 the blade cannot continue with another trial after the impact. This could lead to installation delays
682 and loss of favourable weather windows, and thus, from a conservative approach, it is recommended
683 to not allow any damages in the blade laminate at the root during impact. Thus, for all the load
684 cases considered in this study, only EC-IV is found to be an acceptable sea state for the mating
685 operation from structural damage criteria.

686 **7. Limitation and future work**

687 In the current work, the impact assessment of wind turbine blade root during an offshore
688 mating process was investigated. Certain assumptions and simplifications were made during the
689 numerical modelling. The jack-up crane vessel was not modelled in multi-body simulations, and
690 the crane tip was considered rigidly fixed. However, the jack-up crane vessel's motion can have
691 eigen period in the range of 0.4 - 3 s [49], and can have wave-induced crane tip motions particularly
692 in short waves. Further, depending on the distance between the jack-up legs and the monopile, the
693 presence of jack-up crane vessels during installation may have diffraction effects on the wave loads
694 applied on the monopile. It is interesting to investigate such effects in future. Also, for defining
695 the monopile-soil interaction, only $p - y$ curve was considered in the study, as the horizontal
696 resistance of the soil govern the critical responses in the hub. The $t - z$ and $q - z$ curves which
697 describes the soil-skin friction and end-bearing resistance of the soil respectively will have limited
698 effect and were not included in the study. However, for practical offshore installation sites, soil
699 surveys are thoroughly conducted and $t - z$ and $q - z$ curves are also available for design purposes.
700 Therefore, it is interesting to include these curves in the numerical model and investigate the
701 dynamic responses of the system. Finally, in the finite element analysis, the damage assessment
702 results were investigated on a homogenised root laminate. However, in the future, a progressive
703 failure analysis with emphasis on delamination modelling must be considered.

704 Acknowledgement

705 This work was made possible through the SFI MOVE projects supported by the Research Coun-
706 cil of Norway, NFR project number 237929. The authors would also like to thank the anonymous
707 reviewer for thoughtful comments and suggestions.

References

- [1] L. Li, Z. Gao, T. Moan, Operability analysis of monopile lowering operation using different numerical approaches, International Society of Offshore and Polar Engineers (ISOPE), 2016.
- [2] A. S. Verma, N. P. Vedvik, Z. Gao, Numerical assessment of wind turbine blade damage due to contact/impact with tower during installation, in: IOP Conference Series: Materials Science and Engineering, Vol. 276, IOP Publishing, 2017, pp. 012–025.
- [3] I. Pineda, P. Tardieu, The european offshore wind industry – key trends and statistics 2016, <https://windeurope.org/about-wind/statistics/offshore/european-offshore-wind-industry-key-trends-and-statistics-2016/> (Accessed: -06-01).
- [4] Wind Europe, The European offshore wind industry–Key trends and statistics 2017, Technical Report.
- [5] G. Corbetta, A. Mbistrova, A. Ho, J. Guillet, I. Pineda, The European offshore wind industry–key trends and statistics 2013, European Wind Energy Association (2014) 4–13.
- [6] D. K. Groot, A Novel Method for Installing Offshore Wind Turbine Blades with a Floating Vessel, Master Thesis, TU Delft (2015).
- [7] A. Verma, P. Haselbach, N. Vedvik, Z. Gao, A Global-local damage assessment methodology for impact damage on offshore wind turbine blades during lifting operations (Accepted), 37th International Conference on Ocean, Offshore and Arctic Engineering OMAE (2018).
- [8] S. Darius, GE unveils market-changing 12MW offshore wind turbine, <http://www.rechargenews.com/wind/1443296/ge-unveils-market-changing-12mw-offshore-wind-turbine> (Accessed: 2018-03-01).

- [9] A. S. Verma, Y. Zhao, N. P. Vedvik, Z. Gao, Explicit structural response-based methodology for assessment of operational limits for single blade installation for offshore wind turbines, 4th ICOE2018, Springer Publications.
- [10] H. S. Toft, K. Branner, P. Berring, J. D. Sørensen, Defect distribution and reliability assessment of wind turbine blades, *Engineering Structures* 33 (1) (2011) 171–180.
- [11] A. S. Verma, N. P. Vedvik, Z. Gao, Comprehensive numerical investigation of impact behavior of an offshore wind turbine blade due to impact/contact during installation, Under review in *Ocean Engineering*.
- [12] Z. Jiang, The impact of a passive tuned mass damper on offshore single-blade installation, *Journal of Wind Engineering and Industrial Aerodynamics* 176 (2018) 65–77.
- [13] <https://www.power-technology.com/projects/lake-winds-energy-mason-county-michigan/attachment/lake-winds-energy-mason-county-michigan6/>, Picture.
- [14] Z. Jiang, Z. Gao, Y. Ren, Zhengru Li, D. Lei, A parametric study on the blade final installation process for monopile wind turbines under rough environmental conditions, *Engineering Structures* 172 (201) (2018) 1042–1056.
- [15] Eric Van Buren, Private communication with Eric Van Buren, Fred. Olsen Windcarrier (Accessed: April 18, 2018).
- [16] S. Habali, I. Saleh, Local design, testing and manufacturing of small mixed airfoil wind turbine blades of glass fiber reinforced plastics: part I: design of the blade and root, *Energy conversion and management* 41 (3) (2000) 249–280.
- [17] M. Peeters, G. Santo, J. Degroote, W. V. Paepegem, The concept of segmented wind turbine blades: A review, *Energies* 10 (8) (2017) 1112.
- [18] P. Brøndsted, R. P. Nijssen, *Advances in wind turbine blade design and materials*, Elsevier, 2013.
- [19] S. Ketele, Detailed modeling of connections in large composite wind turbine blades, Master’s thesis, Universiteit Gent (2013).

- [20] V. Martínez, A. Güemes, D. Trias, N. Blanco, Numerical and experimental analysis of stresses and failure in t-bolt joints, *Composite structures* 93 (10) (2011) 2636–2645.
- [21] A. J. A. Briggs, Z. Y. Zhang, H. N. Dhakal, Study on T-bolt and pin-loaded bearing strengths and damage accumulation in E-glass/epoxy blade applications, *Journal of Composite Materials* 49 (9) (2015) 1047–1056.
- [22] B. M. Eriksen, Wind and tidal turbine blade root connection, Master’s thesis, Norwegian University of Science and Technology (NTNU), Trondheim (2011).
- [23] I. G. Mollà, Installing a blade in a wind turbine and wind turbines, US Patent App. 14/657,307 (Oct. 1 2015).
- [24] T. J. Larsen, A. M. Hansen, How 2 HAWC2, the user’s manual, Tech. rep., Risø National Laboratory (2007).
- [25] L. Kuijken, Single Blade Installation for Large Wind Turbines in Extreme Wind Conditions, Master Thesis, Technical University of Denmark (2015).
- [26] J. Velarde, Design of monopile foundations to support the DTU 10 MW offshore wind turbine, Master thesis, Norwegian University of Science and Technology (NTNU), Trondheim (2016).
- [27] M. Damgaard, L. B. Ibsen, L. V. Andersen, J. K. Andersen, Cross-wind modal properties of offshore wind turbines identified by full scale testing, *Journal of Wind Engineering and Industrial Aerodynamics* 116 (2013) 94–108.
- [28] R. Shirzadeh, C. Devriendt, M. A. Bidakhvidi, P. Guillaume, Experimental and computational damping estimation of an offshore wind turbine on a monopile foundation, *Journal of Wind Engineering and Industrial Aerodynamics* 120 (2013) 96–106.
- [29] C. Bak, F. Zahle, R. Bitsche, T. Kim, A. Yde, L. C. Henriksen, M. H. Hansen, A. Natarajan, Description of the DTU 10 MW reference Wind Turbine, Progress report Report-I-0092, DTU Wind Energy (2013).
- [30] O. Faltinsen, Sea loads on ships and offshore structures, Cambridge university press, 1993.
- [31] J. Morison, J. Johnson, S. Schaaf, et al., The force exerted by surface waves on piles, *Journal of Petroleum Technology* 2 (05) (1950) 149–154.

- [32] Norge, Standard, NOR-SOK-N003: Actions and actions effects (2007).
- [33] J. Mann, The spatial structure of neutral atmospheric surface-layer turbulence, *Journal of Fluid Mechanics* 273 (1994) 141–168.
- [34] S. F. Hoerner, *Fluid-dynamic drag: practical information on aerodynamic drag and hydrodynamic resistance*, Hoerner Fluid Dynamics Midland Park, NJ, USA, 1965.
- [35] International Electrotechnical Commission, IEC 614001 Wind Turbine Part 1: Design Requirements. 3rd ed. edn., Geneva, Switzerland (2007).
- [36] K. Hasselmann, Measurements of wind wave growth and swell decay during the joint north sea wave project (jonswap), *Deutschen Hydrografischen Zeitschrift* 8 (1973) 95.
- [37] <https://www.ineffableisland.com/2012/10/wow-worlds-largest-wind-turbine-blade.html>, Picture.
- [38] H. Hibbitt, B. Karlsson, P. Sorensen, *Abaqus analysis users manual version 2016*.
- [39] N. Tanlak, F. Sonmez, E. Talay, Detailed and simplified models of bolted joints under impact loading, *The Journal of Strain Analysis for Engineering Design* 46 (3) (2011) 213–225.
- [40] J.-S. Chou, Y.-C. Ou, K.-Y. Lin, Z.-J. Wang, Structural failure simulation of onshore wind turbines impacted by strong winds, *Engineering Structures* 162 (2018) 257–269.
- [41] P. Haselbach, R. Bitsche, K. Branner, The effect of delaminations on local buckling in wind turbine blades, *Renewable Energy* 85 (2016) 295–305.
- [42] K. Tavakoldavani, Composite materials equivalent properties in lamina, laminate, and structure levels, Master’s thesis, The University of Texas at Arlington (2014).
- [43] R. Tørnqvist, Design of crashworthy ship structures, PhD Thesis, Kongens Lyngby, Technical University of Denmark. (2003).
- [44] S. Ehlers, A procedure to optimize ship side structures for crashworthiness, *Proceedings of the Institution of Mechanical Engineers, Part M: Journal of Engineering for the Maritime Environment* 224 (1) (2010) 1–11.

- [45] G. Perillo, J. Jørgensen, Numerical/experimental study of the impact and compression after impact on gfrp composite for wind/marine applications, *Procedia Engineering* 167 (2016) 129–137.
- [46] G. Perillo, N. Vedvik, A. Echtermeyer, Numerical and experimental investigation of impact on filament wound glass reinforced epoxy pipe, *Journal of Composite Materials* 49.
- [47] P. P. Camanho, Failure criteria for fibre-reinforced polymer composites, *Secção de Mecânica Aplicada, Departamento de Engenharia Mecânica e Gestão Industrial, Faculdade de Engenharia da Universidade do Porto* (2002).
- [48] Y. Hu, B. Yang, S. D. Nie, G. X. Da, Performance of high strength structural bolts in tension: effects of tolerance classes, in: *International Conference on Performance-based and Life-cycle Structural Engineering*, School of Civil Engineering, The University of Queensland, 2015, pp. 776–781.
- [49] Y. Zhao, Z. Cheng, P. C. Sandvik, Z. Gao, T. Moan, E. Van Buren, Numerical modeling and analysis of the dynamic motion response of an offshore wind turbine blade during installation by a jack-up crane vessel, *Ocean Engineering* 165 (2018) 353–364.